Report

Cell Reports

NAD+ Repletion Rescues Female Fertility during Reproductive Aging

Graphical Abstract

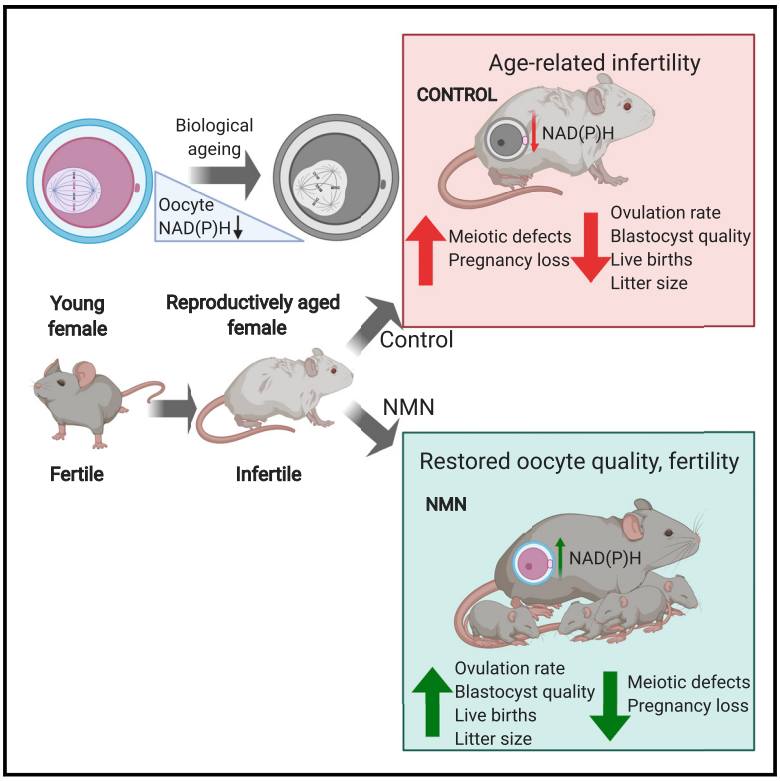

Authors

Michael J. Bertoldo, Dave R. Listijono, Wing-Hong Jonathan Ho, ..., David A. Sinclair, Hayden A. Homer, Lindsay E. Wu

Correspondence

david_sinclair@hms.harvard.edu (D.A.S.), h.homer@uq.edu.au (H.A.H.), lindsay.wu@unsw.edu.au (L.E.W.)

In Brief

Declining oocyte quality is considered an irreversible feature of aging and is rate limiting for human fertility. Bertoldo et al. show that reversing an age-dependent decline in NAD(P)H restores oocyte quality, embryo development, and functional fertility in aged mice. These findings may be relevant to reproductive medicine.

Highlights

- Declining NAD(P)H is associated with oocyte dysfunction during reproductive aging
- Oocyte quality and fertility can be restored by NMN treatment in aged mice
- Supplementation of embryo media with NMN improves developmental milestones
- SIRT2 overexpression mimics benefits of NMN but is unlikely to mediate its effects

Bertoldo et al., 2020, Cell Reports *30*, 1670–1681
February 18, 2020
https://doi.org/10.1016/j.celrep.2020.01.058

CellPress

OPEN ACCESS
CellPress

Cell Reports
Report

NAD+ Repletion Rescues Female Fertility during Reproductive Aging

Michael J. Bertoldo,[1,2,13] Dave R. Listijono,[1,2,13] Wing-Hong Jonathan Ho,[1,2,13] Angelique H. Riepsamen,[2] Dale M. Goss,[1] Dulama Richani,[2] Xing L. Jin,[3] Saabah Mahbub,[4] Jared M. Campbell,[4] Abbas Habibalahi,[4] Wei-Guo Nicholas Loh,[2] Neil A. Youngson,[1] Jayanthi Maniam,[1] Ashley S.A. Wong,[1] Kaisa Selesniemi,[5,6] Sonia Bustamante,[7] Catherine Li,[1] Yiqing Zhao,[2] Maria B. Marinova,[2] Lynn-Jee Kim,[1] Laurin Lau,[2] Rachael M. Wu,[8] A. Stefanie Mikolaizak,[9] Toshiyuki Araki,[10] David G. Le Couteur,[11] Nigel Turner,[1] Margaret J. Morris,[1] Kirsty A. Walters,[2] Ewa Goldys,[4] Christopher O'Neill,[3] Robert B. Gilchrist,[2] David A. Sinclair,[1,5,14,*] Hayden A. Homer,[2,12,14,*] and Lindsay E. Wu[1,14,15,*]

[1]School of Medical Sciences, UNSW Sydney, Sydney, NSW, Australia
[2]School of Women's and Children's Health, UNSW Sydney, Sydney, NSW, Australia
[3]Human Reproduction Unit, Kolling Institute, Sydney Medical School, University of Sydney, St Leonards, NSW, Australia
[4]ARC Centre of Excellence in Nanoscale Biophotonics, UNSW Sydney, NSW, Australia
[5]Paul F. Glenn Laboratories for the Biological Mechanisms of Aging, Harvard Medical School, Boston MA, USA
[6]Jumpstart Fertility Pty Ltd., Sydney, NSW, Australia
[7]Bioanalytical Mass Spectrometry Facility, Mark Wainwright Analytical Centre, UNSW Sydney, Sydney, NSW, Australia
[8]Graduate Entry Medical School, University of Limerick, Limerick, Republic of Ireland
[9]Neuroscience Research Australia, Randwick, NSW, Australia
[10]Department of Peripheral Nervous System Research, National Institute of Neuroscience, National Center of Neurology and Psychiatry, Tokyo, Japan
[11]ANZAC Medical Research Institute, University of Sydney, Concord, NSW, Australia
[12]Christopher Chen Oocyte Biology Laboratory, University of Queensland Centre for Clinical Research, Royal Brisbane & Women's Hospital, Herston, QLD, Australia
[13]These authors contributed equally
[14]These authors contributed equally
[15]Lead Contact
*Correspondence: david_sinclair@hms.harvard.edu (D.A.S.), h.homer@uq.edu.au (H.A.H.), lindsay.wu@unsw.edu.au (L.E.W.)
https://doi.org/10.1016/j.celrep.2020.01.058

SUMMARY

Reproductive aging in female mammals is an irreversible process associated with declining oocyte quality, which is the rate-limiting factor to fertility. Here, we show that this loss of oocyte quality with age accompanies declining levels of the prominent metabolic cofactor nicotinamide adenine dinucleotide (NAD^+). Treatment with the NAD^+ metabolic precursor nicotinamide mononucleotide (NMN) rejuvenates oocyte quality in aged animals, leading to restoration in fertility, and this can be recapitulated by transgenic overexpression of the NAD^+-dependent deacylase SIRT2, though deletion of this enzyme does not impair oocyte quality. These benefits of NMN extend to the developing embryo, where supplementation reverses the adverse effect of maternal age on developmental milestones. These findings suggest that late-life restoration of NAD^+ levels represents an opportunity to rescue female reproductive function in mammals.

INTRODUCTION

Increasing maternal age and subsequent infertility have rapidly become a significant challenge to family planning, as a result of the irreversible decline in female fertility in mammals. The rate-limiting factor for successful pregnancy is oocyte quality, which significantly declines from late in the third decade of life in humans (De Vos et al., 2014; Sauer, 2015). Despite the enormous demand, there are no clinically viable strategies to either preserve or rejuvenate oocyte quality during aging, which is defined by the capacity of the oocyte to support meiotic maturation, fertilization, and subsequent embryonic development. A non-invasive, pharmacological treatment to maintain or restore oocyte quality during aging would alleviate a rate-limiting barrier to pregnancy with increasing age that has driven demand for assisted reproduction technologies (ARTs) such as *in vitro* fertilization (IVF), which is invasive, carries health risks (Kumar et al., 2011), is expensive, and has a limited success rate.

Although somatic tissues undergo continual regeneration through turnover by a self-renewing population of resident precursor stem cells, oocytes in the ovary are laid down during *in utero* development in humans, where they form a finite pool that does not undergo self-renewal. Oocytes are therefore highly susceptible to age-related dysfunction. The molecular basis for the decline in oocyte quality with advancing age implicates genome instability, reduced mitochondrial bioenergetics, increased reactive oxygen species (ROS), and disturbances during meiotic chromosome segregation due to compromised function of the spindle assembly checkpoint (SAC) surveillance system (Franasiak et al., 2014; Greaney et al., 2018). The molecular cause of chromosome mis-segregation in oocytes with advancing age is still unknown, and as a result, there are no

pharmacological strategies to correct this problem. Understanding the molecular or metabolic basis of this defect could lead to therapies that could maintain or even rescue female fertility with advancing age.

The metabolite nicotinamide adenine dinucleotide (NAD^+/NADH) is a prominent redox cofactor and enzyme substrate that is essential to energy metabolism, DNA repair, and epigenetic homeostasis. Levels of this essential cofactor decline with age in somatic tissues (Massudi et al., 2012), and reversing this decline through treatment with metabolic precursors for NAD^+ has gained attention as a treatment for maintaining late-life health (Mills et al., 2016; Rajman et al., 2018). Here, we demonstrate that autofluorescence of NADH and its phosphorylated form NADPH declines in oocytes with age, and we delineate a role for NAD^+ and a potential role for the NAD^+-consuming enzyme SIRT2 as mediators of fertility that are open to pharmacological intervention.

RESULTS

We sought to determine whether NAD^+ declined in oocytes with age, contributing to infertility and declining oocyte quality, and whether this could be reversed through treatment with the NAD^+ precursor nicotinamide mononucleotide (NMN) (Yoshino et al., 2011). To address these questions, we used mice, whose fertility starts to decline around 8 months of age due to oocyte defects that are similar to those in humans (Greaney et al., 2018). Because of the bioanalytical challenges of measuring NAD^+ levels in individual oocytes, we used hyperspectral microscopy imaging techniques that exploit the autofluorescence of NADH and NADPH (Dong et al., 2019; Kolenc and Quinn, 2019). Twelve-month-old females were treated with NMN in drinking water (2 g/L) for 4 weeks, following which mature metaphase-II (MII) oocytes were recovered and subjected to multispectral microscopy imaging of autofluorescence to determine the relative abundances of native fluorophores (Figure 1A). Consistent with our hypothesis, we found that NAD(P)H levels declined in oocytes from aged animals, compared with young (4- to 5-week-old) animals, and NMN treatment increased NAD(P)H levels in oocytes from aged animals (Figure 1B). We next sought to determine whether this trend occurred across the entire ovary, rather than in oocytes alone. Using mass spectrometry, we did not observe a decline in whole ovary NAD(H) levels with age (Figure 1C), suggesting that the oocyte represents an especially vulnerable subunit of the ovary that is subject to an age-related decline in NAD^+, in contrast to the surrounding stroma that makes up the bulk of ovarian tissue. Consistent with data from hyperspectral imaging of individual oocytes, NMN treatment increased NAD^+ levels in the whole ovary, as would be expected following systemic delivery (Figure 1D).

To test whether addressing the age-related decline in oocyte NAD^+ levels would alter oocyte quality, we treated 14-month-old females with NMN in drinking water (2 g/L) for 4 weeks, whereas control animals were maintained on the same drinking water in the absence of NMN. The effects of this intervention on oocyte quality were assessed in germinal vesicle (GV)-stage oocytes collected from the ovaries of pregnant mare's serum gonadotropin (PMSG)-stimulated animals, which were matured *in vitro* to the MII stage, and immunostained to assess spindle structure and chromosome alignment. NMN treatment notably rescued spindle assembly (Figure 2A). Oocyte yield was also increased in aged animals following ovarian hyperstimulation of C57BL/6JAusb mice with PMSG and human chorionic gonadotrophin (hCG) to obtain MII oocytes from the oviduct and hyperstimulation of Swiss albino mice with PMSG alone to obtain GV-stage cumulus oocyte complexes (COCs) directly from punctured ovaries (Figures 2B and 2C). To further test the importance of NAD^+ biosynthesis, we obtained transgenic mouse strains that constitutively overexpress the NAD^+ biosynthetic enzymes NMNAT1 or NMNAT3 (Figures 2D and 2E; Figure S1; Yahata et al., 2009), which are localized to the nucleus or the mitochondria, respectively (Berger et al., 2005). These animals had increased levels of NMNAT1 and NMNAT3 in ovarian tissue, though these proteins could not be detected in oocytes by western blot, most likely because of the low protein concentrations that were obtained from oocytes relevant to other tissues. As with NMN treatment, 12- to 14-month-old *Nmnat1*$^{Tg/+}$ animals, but not *Nmnat3*$^{Tg/+}$ animals, yielded more oocytes than their wild-type littermates (Figures 2D and 2E), suggesting that the subcellular localization of NAD^+ biosynthesis is important for follicular and oocyte function. To test the requirement for NAD^+ biosynthesis in meiotic maturation, we treated GV-stage oocytes with FK866, an inhibitor of the NAD^+ biosynthetic enzyme NAMPT (Hasmann and Schemainda, 2003), and assessed meiotic progression (Figure S2). Both germinal vesicle breakdown (GVBD) and polar body extrusion (PBE) were slowed by FK866 treatment, consistent with the idea that NAD^+ synthesis is essential to oocyte function.

Next, we sought to determine whether late-life NMN treatment resulted in oocytes with improved developmental potential. Twelve-month-old animals were treated with NMN for 4 weeks (2 g/L, drinking water), and MII oocytes were collected from oviducts following PMSG and hCG stimulation. Oocytes from NMN-treated, aged (12-month-old) animals had a larger diameter (Figure 2F), which may be relevant given that oocytes with smaller diameters are associated with poorer outcomes following IVF (Atzmon et al., 2017; Marquard et al., 2011). A separate cohort of oocytes was subjected to IVF, and at day 6, the proportion of embryos that reached blastocyst formation was assessed (Figure 2G), with a trend toward improved blastocyst formation rates. We next sought to determine whether *in vivo* NMN treatment would alter subsequent inner cell mass development of blastocysts, which is highly predictive of pregnancy success (Lane and Gardner, 1997). Twelve-month-old mice were treated with NMN in drinking water for 2, 7, 14, or 28 days, and oocytes subjected to IVF. At day 6, embryos were subjected to differential staining of the inner cell mass. The length of NMN treatment in animals correlated with improvements in inner cell mass size (Figure 2H), and to confirm that this translated to improved fertility outcomes, we treated a cohort of 13-month-old animals with two different doses of NMN (drinking water, 0.5 and 2 g/L) for 4 weeks before the introduction of a male of proven fertility. Breeding performance as determined by pregnancy, live births, and litter size was then assessed for the following 9 weeks, from 14–16 months of age (Figures 2I–2M). NMN treatment improved the time to first live birth (Figure 2J)

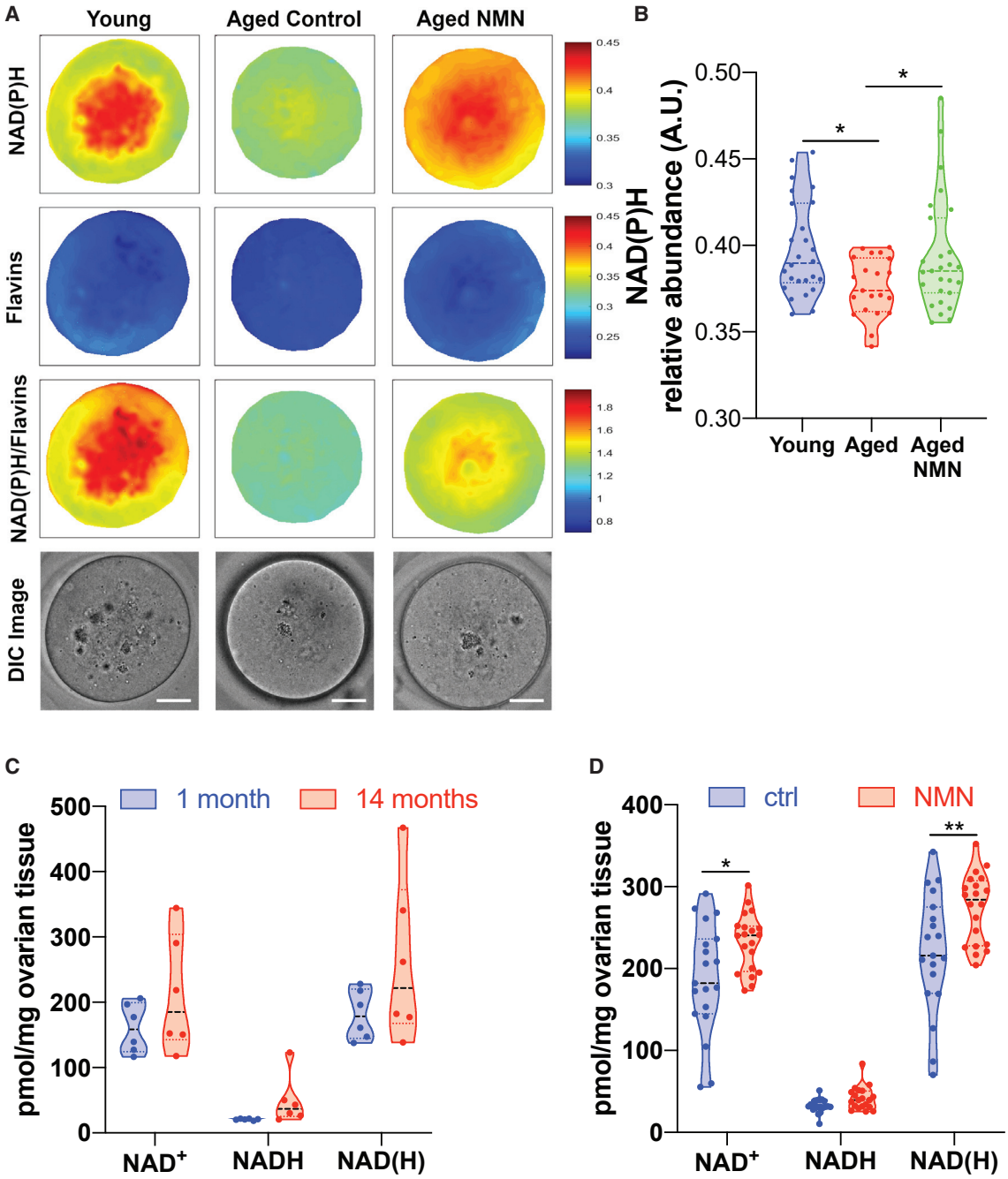

Figure 1. Oocyte NAD$^+$ Levels Decline with Age and Are Increased with NMN Treatment

(A and B) Multispectral imaging (A) to determine NAD(P)H content in oocytes from young (4- to 5-week-old) or aged (12-month-old) mice treated with NMN (drinking water, 2 g/L, 4 weeks) (scale bar is 20 μm), quantified in (B) (one-way ANOVA 1.454 (2, 71), *p = 0.0165, 0.0287 by Dunnett's multiple comparison test, n = 21–27 oocytes per group).

(C and D) Mass spectrometry of the whole ovary (C) shows no change in NAD(H) levels between the ages of 1 and 14 months (n = 6 mice per group); however, (D) NMN increased ovarian NAD(H) in 14-month-old mice (1 h following 400 mg/kg oral gavage, *p = 0.0123, **p = 0.0072, two-tailed t test, n = 20 mice per group).

and the overall proportion of animals achieving live birth during the breeding trial (Figure 2K), though this surprisingly occurred at the lower dose of NMN (0.5 g/L), suggesting that previous experiments were performed at a dose that benefited oocyte quality but may have adversely affected other aspects of fertility. This could be related to an upper limit to NMN tolerability or the increased formation of the NMN degradation product nicotinamide, which is a sirtuin inhibitor (Bitterman et al., 2002). These data from orthogonal pharmacological and genetic approaches show that increasing NAD$^+$ enhances ovulation rate, oocyte

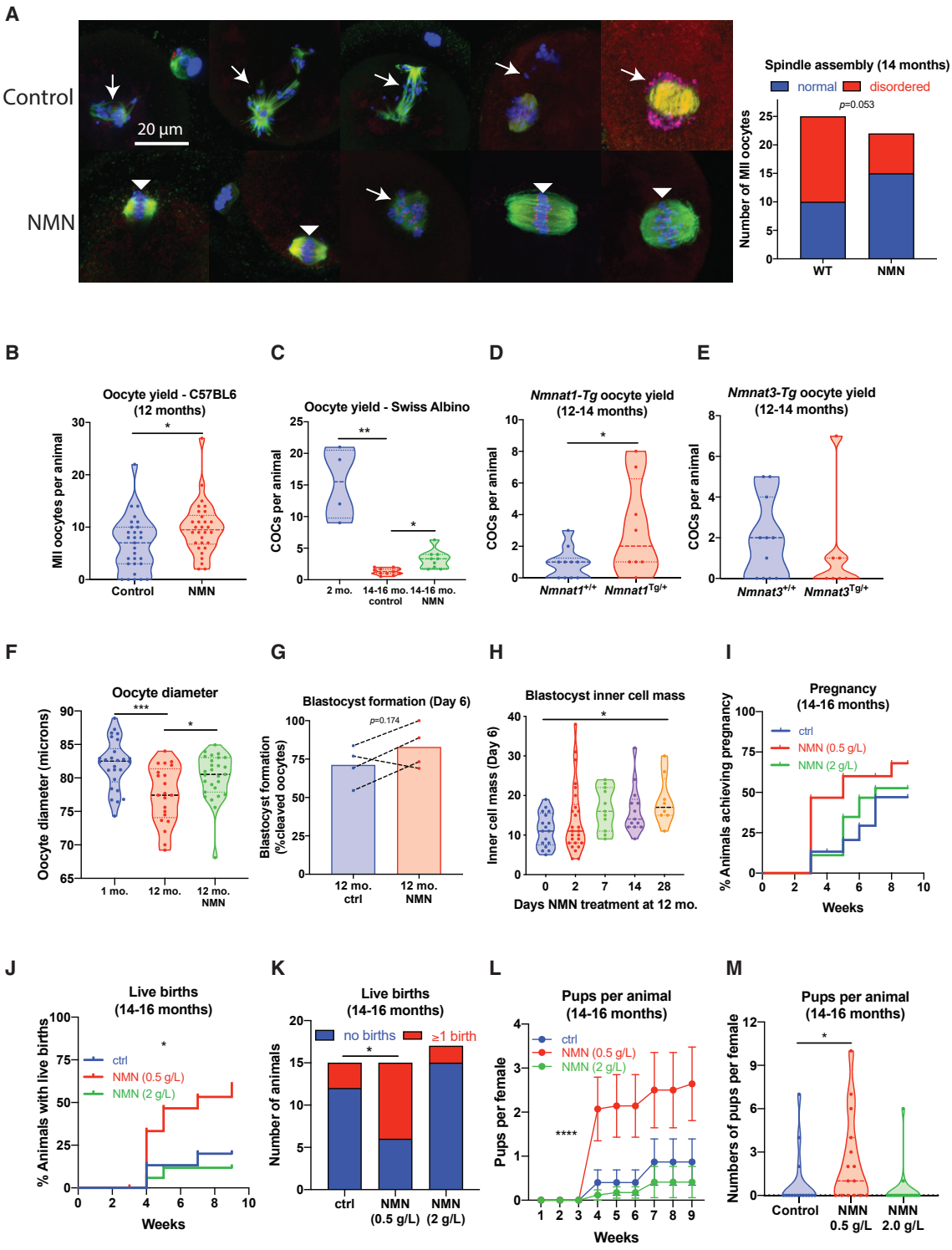

Figure 2. NMN Treatment Restores Oocyte Quality, Follicle Dynamics, Embryo Development, and Live Birth Rates

(A) NMN treatment (drinking water, 2 g/L, 4 weeks) with NMN from 14 months restores spindle assembly in immunostained oocytes (β-tubulin in green, Hoechst for DNA in blue, kinetochores in red, p = 0.0503 by Fisher's exact test, n = 23–25 per group). Disordered spindles with lagging chromosomes are indicated by arrows, and normal, barrel-shaped bipolar spindles with DNA aligned along the metaphase plate are indicated by arrowheads.

(B and C) Oocyte yield following ovarian stimulation in (B) aged (12-month-old) C57BL/6JAusb mice (*p = 0.0211, two-tailed t-test, n = 29–30 animals per group) and (C) 14- to 16-month-old Swiss albino mice (Kruskal-Wallis 16.31, ***p = 0.0004, *p = 0.0295 by Dunnett's mulitple comparison test, n = 4–11 per group).

(legend continued on next page)

quality, and overall live birth rates in aged female mice, though they point to an optimum range of dosing.

Given the potential for clinical translation of this work, it was important to assess whether this treatment would adversely affect the health or development of offspring following maternal NMN exposure. Offspring from a separate cohort of animals maintained on the higher dose of NMN (2 g/L) before mating, during pregnancy, and throughout lactation were maintained on normal chow or challenged with high-fat feeding to determine their health and development. Animals were assessed for physiological and behavioral changes (Figure S3). There were no changes from maternal NMN exposure, except for a small increase in lean body mass from maternal NMN treatment (Figure S3D). These data are in line with recent work (Ear et al., 2019) suggesting that administration of the NAD^+ precursor nicotinamide riboside (NR) during lactation is not harmful and may improve offspring health.

We next sought to determine the mechanism that mediated these benefits. One candidate that we hypothesized for this role is the NAD^+-dependent deacylase SIRT2. We previously showed that SIRT2 stabilizes the SAC protein BubR1 (North et al., 2014), which is critical for meiotic progression (Homer et al., 2009), kinetochore attachment, and chromosome segregation in oocytes (Qiu et al., 2018; Touati et al., 2015; Zhang et al., 2014). Levels of BubR1 decline in mouse reproductive tissue (North et al., 2014) and human oocytes with advancing age (Riris et al., 2014). SIRT2 maintains genome stability through deacetylation of Cdc20 and Cdh1 required for sustaining the activity of the anaphase-promoting complex (Kim et al., 2011), which is an essential oocyte regulator (Homer, 2013; Jin et al., 2010).

To test whether SIRT2 could recapitulate the benefits of NMN treatment, we obtained a strain of $Sirt2^{Tg/+}$ mice (North et al., 2014) that overexpress SIRT2 in all tissues, including oocytes (Figure S4A), and assessed oocyte quality at the age of 14 months. As with our previous experiments, oocytes were immunostained to assess spindle structure and chromosome alignment. As expected, more than 70% of oocytes from reproductively aged wild-type ($Sirt2^{+/+}$) animals had strikingly disordered spindles and poorly aligned chromosomes (Figures 3A and 3B), whereas 80% of oocytes from SIRT2 transgenic ($Sirt2^{Tg/+}$) littermates exhibited normal barrel-shaped bipolar spindles and well-aligned chromosomes. Following stimulation with PMSG, twice as many COCs were obtained from aged $Sirt2^{Tg/+}$ ovaries compared with $Sirt2^{+/+}$ littermates (Figure 3C). Given the importance of spindle integrity and chromosome alignment for chromosome segregation, we next tested whether oocytes from aged $Sirt2^{Tg/+}$ animals might be less prone to aneuploidy, a pathogenomic feature of poor-quality oocytes from aged females. Predictably, aneuploidy rates increased with age, from 15% at 3 months of age to 43% at 16 months of age in $Sirt2^{+/+}$ wild-type oocytes, whereas in oocytes from aged $Sirt2^{Tg/+}$ littermates, the incidence was 20%, comparable to young females (Figure 3D). Oxidative stress is a key driver of oocyte aging and female infertility (Agarwal et al., 2012). SIRT2 deacetylates and maintains the activity of the pentose phosphate pathway enzyme G6PD (Wang et al., 2014), which regenerates the antioxidant glutathione through its production of NADPH. Compared with wild-type oocytes, $Sirt2^{Tg/+}$ oocytes from aged animals displayed markedly reduced levels of ROS, as determined by staining with the ROS-sensitive fluorescent dye H_2DCFDA under both young (5- to 6-month-old) unchallenged (Figures 3E and 3F) and H_2O_2-challenged conditions (Figures S4D and S4E). Consistent with these data and our hypothesis, we observed increased G6PD enzyme activity in $Sirt2^{Tg/+}$oocytes (Figure 3G).

Given the improved characteristics of oocytes from aged $Sirt2^{Tg/+}$ animals, we sought to determine whether this translated into improved fertility. Starting at the age of 15 months, animals were subjected to breeding trials to determine pregnancy rates. Consistent with very low fertility at this age, only 25% of wild-type $Sirt2^{+/+}$ females achieved a pregnancy over 5 mating rounds, whereas this rate tripled to 75% in $Sirt2^{Tg/+}$ females (Figure 3H). These data demonstrate that the NAD^+-dependent deacylase SIRT2 is sufficient to maintain ovarian function and female fertility during aging.

Although these data suggested that SIRT2 was sufficient to recapitulate the benefits of NMN to fertility, we next sought to determine whether SIRT2 was also obligatory for maintaining normal oocyte function through the use of $Sirt2^{-/-}$ knockout animals. Oocytes from whole-body $Sirt2^{-/-}$ knockout mice at the age of 5–6 months displayed normal spindle assembly and maturation (Figure 3I), indicating that at a younger age at which NAD^+ is replete, SIRT2 is not essential for accurate spindle assembly or that redundancy exists in the role of SIRT2 with other yet-to-be-identified factors. These *in vivo* results from *Sirt2* knockout animals are in contrast to *in vitro* studies (Qiu et al., 2018; Riepsamen et al., 2015; Zhang et al., 2014). Altogether,

(D and E) Aged (12- to 14-month-old) transgenic mice overexpressing NMNAT1 have increased oocyte yield (*p = 0.0416, two-tailed t-test, n = 8–10 per group) (D) in comparison to transgenics overexpressing NMNAT3 (n = 7–11) (E).

(F) Oocyte diameter following NMN treatment (2 g/L, drinking water, 4 weeks) in aged (12-month-old) or young (4- to 6-week-old) C57BL/6 females ($F(2,71) = 8.504$, ***p = 0.0002, *p = 0.0332 by Dunnett's multiple comparison test, n = 21–27 oocytes per group).

(G) In a parallel cohort, oocytes were used for IVF, with blastocyst formation at day 6 of embryo development (each datapoint is cumulative data from one independent experiment).

(H) 12-month-old C57BL/6 females were treated for the indicated times with NMN in drinking water (2 g/L), and MII oocytes were subjected to IVF. At day 6, inner cell mass was assessed (Kruskal-Wallis 11.93, *p = 0.0337 by Dunn's multiple comparison test, n = 8–26 oocytes per group). Previously untreated 13-month-old C57BL/6 females (n = 15–17 per group) were treated for 4 weeks with NMN in drinking water at two doses (0.5 and 2 g/L), following which a male was introduced and breeding performance was assessed over the next 9 weeks.

(I–M) Breeding performance was assessed by (I) cumulative time to pregnancy, (J) cumulative time to live birth (log-rank test, **p = 0.0059), (K) overall proportion achieving live birth (Fisher's exact test, *p = 0.0253 ctrl versus 0.5 g/L NMN), (L) cumulative number of pups born over time (repeated-measures ANOVA, NMN $F(2, 43) = 4.925$, p = 0.0119, Dunnett's multiple comparison ctrl versus NMN 0.5, ****p < 0.0001, error bars show SEM), and (M) overall number of pups per female (Kruskal-Wallis 9.220, p = 0.0100, Dunn's multiple comparison, *p = 0.0491 ctrl versus 0.5 g/L NMN).

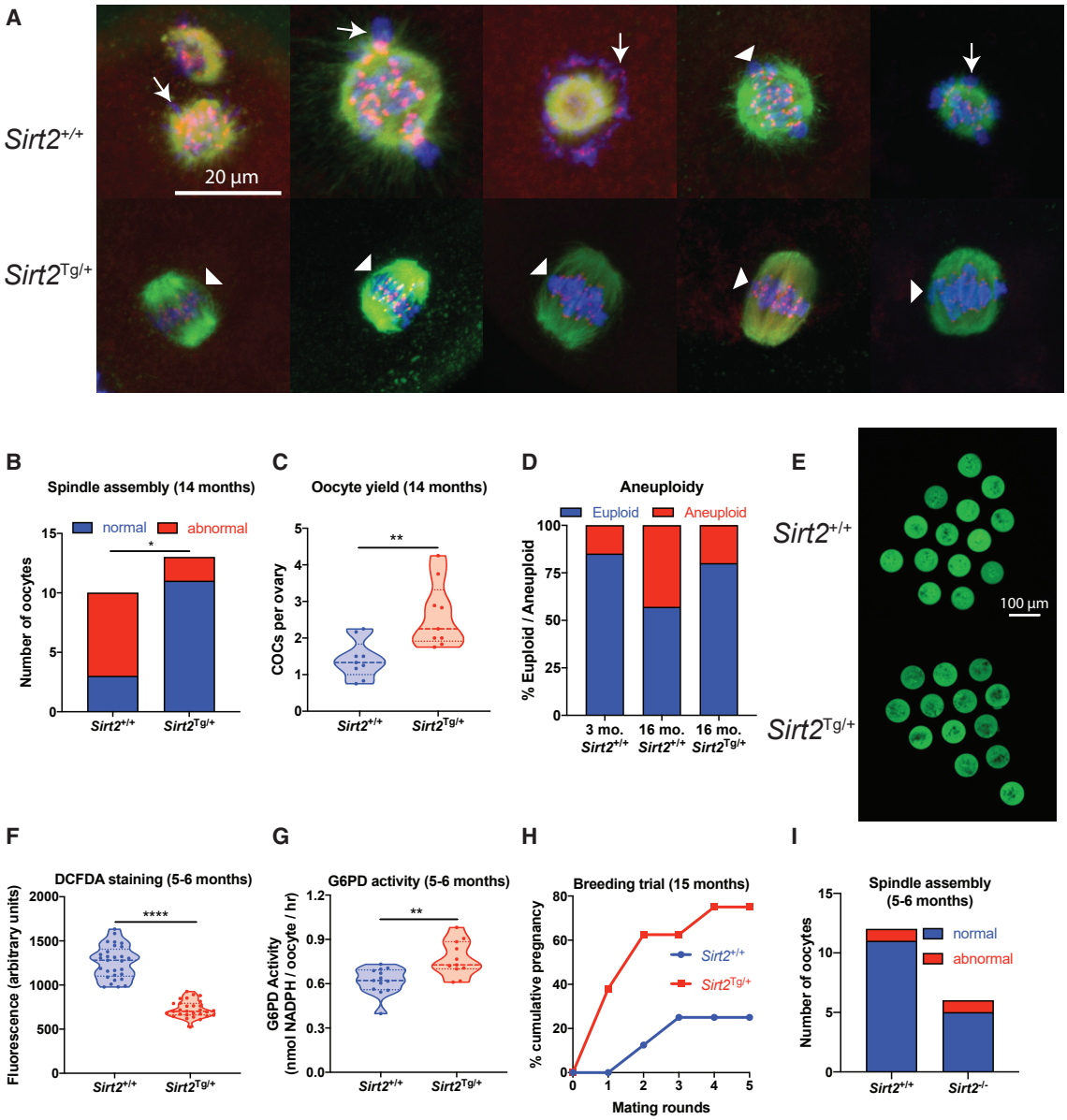

Figure 3. SIRT2 Transgenic Mice Have Improved Oocyte Quality

(A and B) Oocytes from 14-month-old *Sirt2*$^{Tg/+}$ C57BL/6 mice were subjected to (A) immunostaining for spindle assembly (β-tubulin in green, Hoechst for DNA in blue, kinetochores in red). Disordered spindles with lagging chromosomes are indicated by arrows, and normal, barrel-shaped bipolar spindles with DNA aligned along the metaphase plate are indicated by arrowheads; this is quantified in (B) ($p = 0.0131$, n = 10–13 oocytes per group, Fisher's exact test).

(C) Oocyte yield from aged (14-month-old) *Sirt2*$^{Tg/+}$ and wild-type *Sirt2*$^{+/+}$ littermates (**$p = 0.0030$, two-tailed t-test, n = 9 animals per group).

(D) Aneuploidy rates in oocytes from young (2-month-old) and aged (16-month-old) *Sirt2*$^{Tg/+}$ and *Sirt2*$^{+/+}$ littermates (n = 26 young, n = 5–7 aged).

(E–G) Oocytes from *Sirt2*$^{Tg/+}$ mice had decreased ROS levels as determined by (E) H_2DCFDA staining, quantified in (F) (****$p < 0.0001$, two-tailed t-test, n = 29 oocytes per group), with (G) increased G6PD enzyme activity (**$p = 0.0019$, two-tailed t-test, n = 11–13 using 5 pooled oocytes per sample from 4 animals per group).

(H) Mating trials from 15 months of age to determine cumulative pregnancy rates ($p = 0.1319$ after 5 mating rounds, n = 8 animals per group, Fisher's exact test).

(I) Spindle assembly in oocytes from *Sirt2*$^{-/-}$ knockout animals (n = 6, 14 oocytes per group).

these data suggest that SIRT2 is sufficient, but not required, to improve oocyte quality during aging.

Next, we asked whether elevating NAD^+ might also benefit pre-implantation embryo development. To test this, IVF was performed using *in vivo* matured oocytes from reproductively aged (12-month-old) or young (4-week-old) females. Following IVF, embryos were cultured in the presence or absence of NMN. Supplementation with NMN improved blastocyst formation in embryos derived from oocytes from aged females (Figure 4A), but not in embryos arising from oocytes from young females (Figures

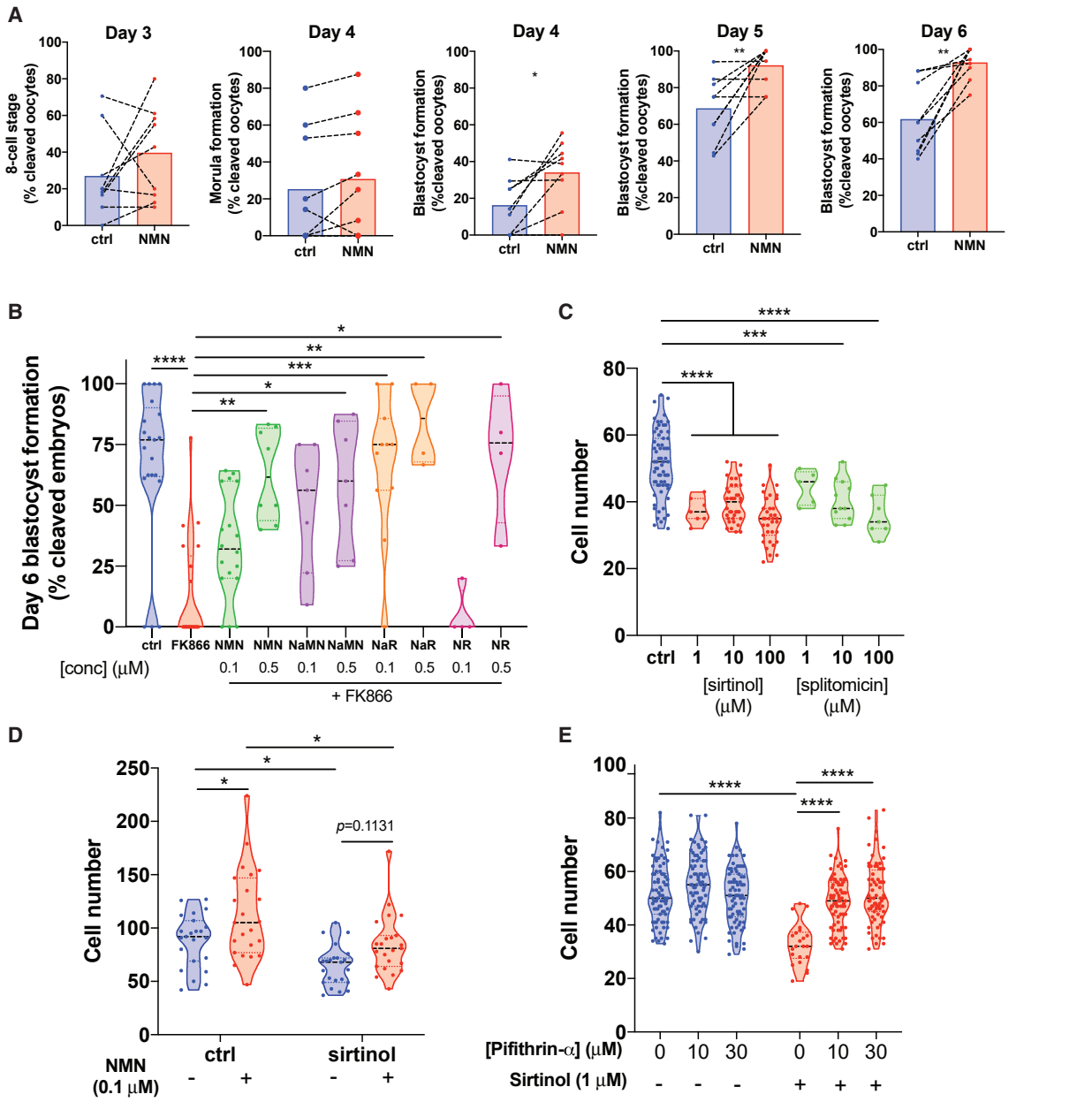

Figure 4. *In Vitro* NMN Treatment Enhances Embryo Formation

(A) Oocytes from aged (12-month-old) mice were subjected to IVF, and embryos maintained in 1 μM NMN until day 6 of embryo development (paired two-tailed t test, day 4 *p = 0.0138, day 5 **p = 0.0086, day 6 **p = 0.0014, n = 9 independent experiments).

(B) Treatment with the NAMPT inhibitor FK866 causes embryo death at day 6, which can be rescued by the NAD^+ precursors NMN, nicotinic acid mononucleotide (NaMN), nicotinic acid riboside (NaR), and NR (Kruskal-Wallis 50.65, p < 0.0001, ****p < 0.0001, **p = 0.0048, *p = 0.0197, ***p = 0.0004, **p = 0.0014, *p = 0.0156, n = 4–21 embryos per group as shown).

(C) Treatment with sirtinol or splitomicin inhibits blastocyst formation (supplemental), with decreased cell count in blastocysts (one-way ANOVA F(6,162) = 22.44, ***p = 0.0002, ****p < 0.0001 by Dunnett's multiple comparison test, n = 5–67 per group as shown by raw datapoints).

(D) Co-treatment of sirtinol-treated embryos with NMN rescues this reduction (two-way ANOVA F(1,88) sirtinol = 17.66, NMN = 12.59, *p = 0.0360, 0.0374, ****p < 0.0001 by Sidak's multiple comparison test, n = 22–23 per group).

(E) Treatment with the p53 inhibitor pifithrin rescues cell count and blastocyst formation (supplemental) in embryos treated with sirtinol (pifithrin F(2,392) = 22.37, sirtinol F(1,392) = 49.81, ****p < 0.0001 by Sidak's multiple comparison test, n = 72–78 per group).

S5A and S5B). To further assess whether NMN could rescue embryo development under challenged conditions, embryos from young animals were maintained in a simple culture medium that accentuates culture stress and restricts embryo development (Li et al., 2012). Consistent with results from aged animals, the addition of NMN to simple media improved blastocyst cell number, an indicator of implantation success (Figure S5C).

Mammalian cells have the capacity to generate NAD^+ via several biosynthetic routes and intermediate precursors (Figure S6; Bieganowski and Brenner, 2004; Nishizuka and Hayaishi, 1963; Okuno and Schwarcz, 1985; Preiss and Handler, 1958a, 1958b). To assess whether NAD^+ synthesis via endogenous NMN production in the recycling pathway plays a role in embryo development, we cultured embryos in the presence of the NAMPT inhibitor FK866 (Hasmann and Schemainda, 2003), which induced blastocyst degeneration on day 6 of culture (Figure S5D). This could be rescued by NMN cotreatment (Figure 4B), as well as other NAD^+ precursors (Figure 4B). In contrast, treatment with the Priess Handler enzyme nicotinic acid phosphoribosyltransferase (NaPRT) inhibitor 2-hydroxynicotinic acid (Piacente et al., 2017) did not affect embryo development (Figures S5E, S5F, and S6).

We next sought to determine whether NMN treatment mediated benefits via the sirtuins. The small-molecule sirtuin inhibitors sirtinol (Grozinger et al., 2001) and splitomicin (Bedalov et al., 2001) impaired embryo growth under simple defined media conditions (Li et al., 2012; Figure 4C; Figure S5G), and this decline in embryo cell number was partially reversed by NMN cotreatment (Figure 4D), suggesting that the sirtuins are not the primary target of NMN in enhancing preimplantation embryo development. This interpretation is clouded by the absence of data to confirm that sirtinol offered complete inhibition of its targets, because only partial inhibition could result in some of the target using increased NAD^+ to rescue embryo development.

Given the ability of sirtuin inhibitors to reduce blastocyst quality, we next sought to determine the pathway through which these inhibitors restrict embryo growth. The most prominently studied member of the sirtuins, SIRT1, deacetylates p53 to inhibit its activity and prevent apoptosis (Cheng et al., 2003; Vaziri et al., 2001). p53 activity is increased in embryos produced by IVF compared with *in vivo*-derived embryos, likely due to culture stress, and its genetic deletion overcomes the effects of culture on blastocyst development (Li et al., 2007, 2012). Activation of p53 is detrimental, because it inhibits proliferation and induces apoptosis of the inner cell mass, which goes on to form the developing fetus (Ganeshan et al., 2010, 2017; Kawamura et al., 2010). We observed that treatment with the p53 inhibitor pifithrin (Komarov et al., 1999) overcame sirtinol-mediated reduction in cell number (Figure 4E) and blastocyst development (Figure S5H), suggesting that p53-dependent hypotrophy is sirtuin mediated (Peck et al., 2010).

DISCUSSION

There is an ongoing trend across the developed world to defer pregnancy until later in life, leading to a steady increase in demand for ARTs. Despite maternal age being the greatest clinical challenge for reproductive medicine, there are no therapeutic treatments to improve oocyte quality. In the current study, we show that oocyte levels of NAD(P)H decline with age and demonstrate that NAD^+ repletion using NMN restores oocyte quality and enhances ovulation rate and fertility. Furthermore, supplementation of NMN in embryo culture media reversed the adverse effects of age on development.

The present study supports the premise that age-related reductions in NAD^+ availability are a determinant of declining oocyte quality and female infertility and that pharmacological restoration of NAD^+ opens a therapeutic window for the treatment of age-related infertility. Several questions remain, including how NMN treatment would restore oocyte quality in aged animals. One well-known consequence of poor oocyte quality with advancing age is chromosome segregation defects, which overwhelmingly affect the first meiotic division (MI). Indeed, 80%–90% of age-related embryonic aneuploidy is the consequence of female MI errors (Greaney et al., 2018). The ability to segregate chromosomes accurately depends upon multiple factors that critically include proper spindle assembly and surveillance of chromosome segregation by the SAC, which we and others have shown is critical for preventing aneuploidy in oocytes (Homer et al., 2005). Adequate expression of key regulatory factors including SAC proteins is determined during a protracted growth phase that the oocyte undergoes concomitant with follicle development within the ovary; it is during this growth phase that the oocyte is transcriptionally and translationally active and stockpiles the reserves required for oocyte maturation and early embryonic divisions for when both transcription and translation have shut down (Greaney et al., 2018). This is a bioenergetically demanding process, and ATP consumption is maximal in mouse oocytes during the spindle assembly phase in MI (Dalton et al., 2014). In mouse oocytes, this growth phase lasts 2–3 weeks before ovulation, whereas we administered NMN for 4 weeks. Although one explanation for improved oocyte quality could be related to increased atresia of suboptimal oocytes before ovulation because of improved quality control mechanisms, we hypothesize that the length of the NMN treatment period improves overall oocyte quality during this critical phase of maturation, with no change in overall sorting or quality control mechanisms, and instead decreases atresia due to improved oocyte quality. It may be that NAD^+ deficiency with age impedes energy metabolism through its requirement as an essential redox cofactor; therefore, treatment with NMN during this critical phase of susceptibility could lower rates of spindle assembly defects and aneuploidy.

Hyperspectral imaging of NADH and NADPH autofluorescence revealed a decline in oocyte NAD(P)H levels with age, whereas mass spectrometry of homogenized, whole ovary did not reveal an age-related decline in NAD(H) levels. This may be related to the increased age of oocytes, which in most mammals are formed during *in utero* development and do not undergo turnover in adult life, with these cells being older than surrounding somatic cells. It would be ideal to measure NAD(H) levels in individual oocytes by mass spectrometry as a complementary technique, because our inability to accurately assay NAD metabolites by mass spectrometry at the single-cell level is a limitation of this study.

One unexpected aspect of this study was that treatment with a lower dose of NMN resulted in improved functional fertility, as

assessed by pregnancy and live birth in aged animals. This could suggest that there is an optimum range for dosing of NAD^+ precursors beyond which other aspects of fertility could be adversely affected, lowering functional fertility. This will be an important concern to the clinical translation of this work, especially given that NAD^+ precursors such as NR are freely available as supplements. Out of caution, we suggest that these supplements should not be taken by women wishing to become pregnant until further studies have been completed.

The present study implicates the NAD^+ metabolome in regulating ovulation rate. We hypothesize that this change in ovulation results from decreased atresia of follicles during maturation, during which oocytes exhibit susceptibilities, as described earlier, rather than change to ovarian reserve. We do not exclude the possibility that NMN exerts benefits to follicular development through direct interactions with tissues other than the ovary, because we delivered NMN through systemic dosing. Furthermore, other tissues may also be susceptible to an age-related decline in NAD^+.

Although NAD^+ is a prominent molecule used as a cofactor or substrate across a range of reactions, we sought to determine whether the benefits of NMN to oocyte integrity might be mediated partly by the NAD^+-dependent deacylase SIRT2. The benefits of *in vivo* NMN treatment could largely be recapitulated by transgenic overexpression of *Sirt2* in aged animals, although its constitutive deletion had no adverse impact on oocyte quality, at least in the younger animals studied here. SIRT2 plays a role in the maintenance of microtubule-kinetochore attachments through its deacetylation and stabilization of BubR1 (North et al., 2014; Qiu et al., 2018), a process that safeguards fidelity in chromosome separation by ensuring the bipolar orientation of chromosomes to the spindle. Consequently, in oocytes from $Sirt2^{Tg/+}$-overexpressing animals, increases in kinetochore-microtubule stability may have contributed to augmented chromosome alignment and improved fertility. These observations are in agreement with separate *in vitro* studies in which chemical or morpholino-mediated *Sirt2* knockdown in oocytes resulted in severe spindle defects and chromosome disorganization (Qiu et al., 2018; Riepsamen et al., 2015). In contrast to those studies, we observed that oocytes from constitutive *Sirt2* knockout mice maintained normal spindle assembly and chromosome organization, suggesting that SIRT2 may be dispensable for oocytes. This interpretation is limited by the young age of knockout animals in that experiment; the only way to definitively determine whether SIRT2 mediates the benefits of NMN in fertility would be to test NMN treatment in aged (12- to 14-month-old) *Sirt2* knockout mice. Another limitation of this study was that we did not measure ROS or G6PD activity in oocytes from these knockout animals. These data suggest the existence of overlapping mechanisms that may compensate during development. Other members of the sirtuins family have been implicated in oocyte development (Tatone et al., 2018; Zhang et al., 2016), and further studies could aim to investigate whether these members are involved in mediating the benefits of NMN treatment observed here. Overall, our data do not yet suggest a role for SIRT2 in mediating the benefits of increased NAD. Increasing NAD^+ levels could instead be affecting oocytes by simply enhancing energy metabolism.

Having demonstrated that *in vivo* NMN treatment in aged animals improved oocyte quality and increased ovulation rate and birth rates, we next showed that supplementing embryo culture media with NMN improved embryo development in embryos derived from oocytes from aged animals, but not young animals, supporting the idea that this intervention addresses an age-related deficit in oocyte NAD^+ levels. This finding is highly relevant to the clinical practice of IVF. In addition to age-related issues of decreased oocyte numbers and oocyte quality, mitotic aneuploidy (Munné et al., 2002) and poor preimplantation embryo development (Janny and Menezo, 1996) limit the number of euploid blastocysts available for transfer with increasing maternal age. The increasing preference for blastocyst-stage transfers in clinical IVF underscores the importance of reaching more advanced developmental milestones (National Perinatal Epidemiology and Statistics Unit, 2016) and clinical demand for interventions that can improve embryo development.

Although this study used NMN as an NAD^+ precursor, alternative precursors from other pathways also raise NAD^+, most notably NR (Trammell et al., 2016). We anticipate that this and similar compounds will also exhibit efficacy in oocyte quality and fertility, and it is unlikely that these effects are unique to NMN.

This work represents a clinically tractable pharmacological intervention to non-invasively treat female infertility caused by a loss of oocyte viability in reproductively aged females, with important clinical implications. We envisage this work could lead to the development of orally delivered therapeutics that enhance oocyte quality for natural conception or IVF. Moreover, this work could enhance the success rates of existing IVF protocols by improving embryo culture conditions and developmental outcomes. Any intervention that improves fertility would lead to cost savings and lower the emotional stress of failed IVF rounds or infertility that can lead to long term psychological and social issues, including depression and relationship breakdown. This could represent an intervention that enables women with poor oocyte quality to have children with their own genetic makeup, because currently, these women have no alternative but to use donated oocytes. Future studies should aim to test NAD^+-raising compounds in a clinical setting, both as an oral therapeutic and as an additive to embryo media, to assess the relevance of these findings to human infertility. While promising, we caution against the use of NAD^+-raising supplements until these clinical studies have been completed.

STAR★METHODS

Detailed methods are provided in the online version of this paper and include the following:

- KEY RESOURCES TABLE
- LEAD CONTACT AND MATERIALS AVAILABILITY
- EXPERIMENTAL MODEL AND SUBJECT DETAILS
- METHOD DETAILS
  - Ovarian stimulation, oocyte collection for *in vitro* maturation and spindle assessment (Figures 1 and 2)
  - Monastrol treatment and ploidy assessment
  - Oocyte collection and confocal imaging – DCFDA staining

SUPPLEMENTAL INFORMATION

Supplemental Information can be found online at https://doi.org/10.1016/j.celrep.2020.01.058.

ACKNOWLEDGMENTS

Funding by the National Health and Medical Research Council (NHMRC) of Australia (APP1103689, APP1122484, APP1139763, APP1044295, APP1066172, and APP1127821) and the Australian Research Council (ARC) (DP170101863 and CE140100003). Salary and experimental costs of M.J.B. and D.M.G. working in the lab of R.B.G. and L.E.W. were partly supported by sponsored research contracts from Jumpstart Fertility to UNSW. K.S. was an employee of Jumpstart Fertility. We gratefully acknowledge assistance from the UNSW Biological Resource Centre. The graphical abstract for this paper was created using BioRender. We wish to thank anonymous donors for their philanthropic support.

AUTHOR CONTRIBUTIONS

L.E.W., H.A.H., and D.A.S. conceived of this study and obtained funding. L.E.W., H.A.H., D.A.S., R.B.G., K.A.W., C.O., M.J.M., and E.G. designed and supervised experiments and analyzed and interpreted results. W.-H.J.H., D.R.L., M.J.B., D.M.G., A.H.R., K.S., W.-G.N.L., A.S.A.W., D.R., C.L., J.M., N.A.Y., L.L., R.M.W., L.-J.K., S.B., X.J.L., S.M., J.M.C., A.H., and M.B.M. carried out experiments and analyzed results. T.A. generated *Nmnat3* transgenic mice. A.S.M. assisted in statistical analysis. N.T. and D.G.L.C. provided critical feedback. L.E.W. wrote and prepared this manuscript.

DECLARATION OF INTERESTS

L.E.W., H.A.H., and D.A.S. are cofounders, shareholders, directors, and advisers of Jumpstart Fertility Inc., which was founded to develop the work described here, and are inventors on a patent (WO2019023748A1 "Methods to improve fertility") that forms the basis of this work and has been licensed to Jumpstart Fertility. D.A.S. is an inventor on a patent (WO2013002880A1) that was previously licensed to Jumpstart Fertility. The salaries of M.J.B. and D.M.G. working in the labs of L.E.W. and R.B.G. at UNSW were paid by sponsored research from Jumpstart Fertility to UNSW. K.S. was an employee of Jumpstart Fertility. W.-H.J.H. and D.R.L. hold shares in Jumpstart Fertility. H.A.H. undertakes ART in the private sector in affiliation with Queensland Fertility Group. L.E.W. and D.A.S. are also advisers and shareholders in EdenRoc Sciences (Metro Biotech NSW, Metro Biotech, Liberty Biosecurity) and in Life Biosciences LLC and its daughter companies (Jumpstart Fertility, Continuum Biosciences, Senolytic Therapeutics, Selphagy, Animal Biosciences, Iduna). L.E.W. provides consulting work for Life Biosciences and is an adviser and shareholder in Intravital Pty Ltd. D.A.S. is also a founder, equity owner, adviser, director, consultant, investor, and/or inventor on patents licensed to Vium, Jupiter Orphan Therapeutics, Cohbar, Galilei Biosciences, Wellomics, EdenRoc Sciences (and affiliates Arc-Bio, Dovetail Genomics, Claret, Revere Biosciences, UpRNA, MetroBiotech, Liberty Biosecurity), Life Biosciences (and affiliates Selphagy, Senolytic Therapeutics, Spotlight Therapeutics, Animal Biosciences, Iduna, Continuum, Jumpstart Fertility, Iduna). D.A.S. is an inventor on a patent application filed by Mayo Clinic and Harvard Medical School that has been licensed to Elysium Health. For details see https://genetics.med.harvard.edu/sinclair.

Received: September 12, 2019
Revised: November 3, 2019
Accepted: January 17, 2020
Published: February 11, 2020

REFERENCES

Agarwal, A., Aponte-Mellado, A., Premkumar, B.J., Shaman, A., and Gupta, S. (2012). The effects of oxidative stress on female reproduction: a review. Reprod. Biol. Endocrinol. *10*, 49.

Atzmon, Y., Shoshan-Karchovsky, E., Michaeli, M., Aslih, N., Shrem, G., Ellenbogen, A., and Shalom-Paz, E. (2017). Obesity results with smaller oocyte in *in vitro* fertilization/intracytoplasmic sperm injection cycles-a prospective study. J. Assist. Reprod. Genet. *34*, 1145–1151.

Bedalov, A., Gatbonton, T., Irvine, W.P., Gottschling, D.E., and Simon, J.A. (2001). Identification of a small molecule inhibitor of Sir2p. Proc. Natl. Acad. Sci. USA *98*, 15113–15118.

Berger, F., Lau, C., Dahlmann, M., and Ziegler, M. (2005). Subcellular compartmentation and differential catalytic properties of the three human nicotinamide mononucleotide adenylyltransferase isoforms. J. Biol. Chem. *280*, 36334–36341.

Bieganowski, P., and Brenner, C. (2004). Discoveries of nicotinamide riboside as a nutrient and conserved NRK genes establish a Preiss-Handler independent route to NAD+ in fungi and humans. Cell *117*, 495–502.

Bitterman, K.J., Anderson, R.M., Cohen, H.Y., Latorre-Esteves, M., and Sinclair, D.A. (2002). Inhibition of silencing and accelerated aging by nicotinamide, a putative negative regulator of yeast sir2 and human SIRT1. J. Biol. Chem. *277*, 45099–45107.

Bustamante, S., Jayasena, T., Richani, D., Gilchrist, R.B., Wu, L.E., Sinclair, D.A., Sachdev, P.S., and Braidy, N. (2017). Quantifying the cellular NAD+ metabolome using a tandem liquid chromatography mass spectrometry approach. Metabolomics *14*, 15.

Cheng, H.L., Mostoslavsky, R., Saito, S., Manis, J.P., Gu, Y., Patel, P., Bronson, R., Appella, E., Alt, F.W., and Chua, K.F. (2003). Developmental defects and p53 hyperacetylation in Sir2 homolog (SIRT1)-deficient mice. Proc. Natl. Acad. Sci. USA *100*, 10794–10799.

Dalton, C.M., Szabadkai, G., and Carroll, J. (2014). Measurement of ATP in single oocytes: impact of maturation and cumulus cells on levels and consumption. J. Cell. Physiol. *229*, 353–361.

De Vos, M., Smitz, J., and Woodruff, T.K. (2014). Fertility preservation in women with cancer. Lancet *384*, 1302–1310.

Dong, Y., Digman, M.A., and Brewer, G.J. (2019). Age- and AD-related redox state of NADH in subcellular compartments by fluorescence lifetime imaging microscopy. Geroscience *41*, 51–67.

Ear, P.H., Chadda, A., Gumusoglu, S.B., Schmidt, M.S., Vogeler, S., Malicoat, J., Kadel, J., Moore, M.M., Migaud, M.E., Stevens, H.E., et al. (2019). Maternal Nicotinamide Riboside Enhances Postpartum Weight Loss, Juvenile Offspring Development, and Neurogenesis of Adult Offspring. Cell Rep. *26*, 969–983.

Franasiak, J.M., Forman, E.J., Hong, K.H., Werner, M.D., Upham, K.M., Treff, N.R., and Scott, R.T., Jr. (2014). The nature of aneuploidy with increasing age of the female partner: a review of 15,169 consecutive trophectoderm biopsies evaluated with comprehensive chromosomal screening. Fertil. Steril. *101*, 656–663.

Ganeshan, L., Li, A., and O'Neill, C. (2010). Transformation-related protein 53 expression in the early mouse embryo compromises preimplantation embryonic development by preventing the formation of a proliferating inner cell mass. Biol. Reprod. *83*, 958–964.

Ganeshan, L., Jin, X.L., and O'Neill, C. (2017). The induction of tumour suppressor protein P53 limits the entry of cells into the pluripotent inner cell mass lineage in the mouse embryo. Exp. Cell Res. *358*, 227–233.

Gosnell, M.E., Anwer, A.G., Cassano, J.C., Sue, C.M., and Goldys, E.M. (2016a). Functional hyperspectral imaging captures subtle details of cell metabolism in olfactory neurosphere cells, disease-specific models of neurodegenerative disorders. Biochim. Biophys. Acta *1863*, 56–63.

Gosnell, M.E., Anwer, A.G., Mahbub, S.B., Perinchery, S.M., Inglis, D.W., Adhikary, P.P., Jazayeri, J.A., Cahill, M.A., Saad, S., and Pollock, C.A. (2016b). Quantitative non-invasive cell characterisation and discrimination based on multispectral autofluorescence features. Sci. Rep. *6*, 23453.

Greaney, J., Wei, Z., and Homer, H. (2018). Regulation of chromosome segregation in oocytes and the cellular basis for female meiotic errors. Hum. Reprod. Update *24*, 135–161.

Grozinger, C.M., Chao, E.D., Blackwell, H.E., Moazed, D., and Schreiber, S.L. (2001). Identification of a class of small molecule inhibitors of the sirtuin family of NAD-dependent deacetylases by phenotypic screening. J. Biol. Chem. *276*, 38837–38843.

Habibalahi, A., Bala, C., Allende, A., Anwer, A.G., and Goldys, E.M. (2019). Novel automated non invasive detection of ocular surface squamous neoplasia using multispectral autofluorescence imaging. Ocul. Surf. *17*, 540–550.

Hasmann, M., and Schemainda, I. (2003). FK866, a highly specific noncompetitive inhibitor of nicotinamide phosphoribosyltransferase, represents a novel mechanism for induction of tumor cell apoptosis. Cancer Res. *63*, 7436–7442.

Homer, H. (2013). The APC/C in female mammalian meiosis I. Reproduction *146*, R61–R71.

Homer, H.A., McDougall, A., Levasseur, M., Yallop, K., Murdoch, A.P., and Herbert, M. (2005). Mad2 prevents aneuploidy and premature proteolysis of cyclin B and securin during meiosis I in mouse oocytes. Genes Dev. *19*, 202–207.

Homer, H., Gui, L., and Carroll, J. (2009). A spindle assembly checkpoint protein functions in prophase I arrest and prometaphase progression. Science *326*, 991–994.

Janny, L., and Menezo, Y.J. (1996). Maternal age effect on early human embryonic development and blastocyst formation. Mol. Reprod. Dev. *45*, 31–37.

Jemiolo, B., Harvey, S., and Novotny, M. (1986). Promotion of the Whitten effect in female mice by synthetic analogs of male urinary constituents. Proc. Natl. Acad. Sci. USA *83*, 4576–4579.

Jin, F., Hamada, M., Malureanu, L., Jeganathan, K.B., Zhou, W., Morbeck, D.E., and van Deursen, J.M. (2010). Cdc20 is critical for meiosis I and fertility of female mice. PLoS Genet. *6*, e1001147.

Kapoor, T.M., Mayer, T.U., Coughlin, M.L., and Mitchison, T.J. (2000). Probing spindle assembly mechanisms with monastrol, a small molecule inhibitor of the mitotic kinesin, Eg5. J. Cell Biol. *150*, 975–988.

Kawamura, Y., Uchijima, Y., Horike, N., Tonami, K., Nishiyama, K., Amano, T., Asano, T., Kurihara, Y., and Kurihara, H. (2010). Sirt3 protects *in vitro*-fertilized mouse preimplantation embryos against oxidative stress-induced p53-mediated developmental arrest. J. Clin. Invest. *120*, 2817–2828.

Keshava, N. (2003). A survey of spectral unmixing algorithms. Linc. Lab. J. *14*, 55–78.

Keshava, N., and Mustard, J.F. (2002). Spectral unmixing. IEEE Signal Process. Mag. *19*, 44–57.

Keshava, N., Kerekes, J.P., Manolakis, D.G., and Shaw, G.A. (2000). Algorithm taxonomy for hyperspectral unmixing. Proceedings of the Algorithms for Multispectral, Hyperspectral, and Ultraspectral Imagery VI *4049*, 42–63.

Kim, H.S., Vassilopoulos, A., Wang, R.H., Lahusen, T., Xiao, Z., Xu, X., Li, C., Veenstra, T.D., Li, B., Yu, H., et al. (2011). SIRT2 maintains genome integrity and suppresses tumorigenesis through regulating APC/C activity. Cancer Cell *20*, 487–499.

Kolenc, O.I., and Quinn, K.P. (2019). Evaluating Cell Metabolism Through Autofluorescence Imaging of NAD(P)H and FAD. Antioxid. Redox Signal. *30*, 875–889.

Komarov, P.G., Komarova, E.A., Kondratov, R.V., Christov-Tselkov, K., Coon, J.S., Chernov, M.V., and Gudkov, A.V. (1999). A chemical inhibitor of p53 that protects mice from the side effects of cancer therapy. Science *285*, 1733–1737.

Kumar, P., Sait, S.F., Sharma, A., and Kumar, M. (2011). Ovarian hyperstimulation syndrome. J. Hum. Reprod. Sci. *4*, 70–75.

Lane, M., and Gardner, D.K. (1997). Differential regulation of mouse embryo development and viability by amino acids. J. Reprod. Fertil. *109*, 153–164.

Li, A., Chandrakanthan, V., Chami, O., and O'Neill, C. (2007). Culture of zygotes increases TRP53 [corrected] expression in B6 mouse embryos, which reduces embryo viability. Biol. Reprod. *76*, 362–367.

Li, A., Ganeshan, L., and O'Neill, C. (2012). The effect of Trp53 gene-dosage and parent-of-origin of inheritance on mouse gamete and embryo function *in vitro*. Biol. Reprod. *86*, 175.

Li, H.J., Sutton-McDowall, M.L., Wang, X., Sugimura, S., Thompson, J.G., and Gilchrist, R.B. (2016). Extending prematuration with cAMP modulators enhances the cumulus contribution to oocyte antioxidant defence and oocyte quality via gap junctions. Hum. Reprod. *31*, 810–821.

Mahbub, S.B., Plöschner, M., Gosnell, M.E., Anwer, A.G., and Goldys, E.M. (2017). Statistically strong label-free quantitative identification of native fluorophores in a biological sample. Sci. Rep. *7*, 15792.

Maniam, J., and Morris, M.J. (2010). Palatable cafeteria diet ameliorates anxiety and depression-like symptoms following an adverse early environment. Psychoneuroendocrinology *35*, 717–728.

Marquard, K.L., Stephens, S.M., Jungheim, E.S., Ratts, V.S., Odem, R.R., Lanzendorf, S., and Moley, K.H. (2011). Polycystic ovary syndrome and maternal obesity affect oocyte size in in vitro fertilization/intracytoplasmic sperm injection cycles. Fertil. Steril. *95*, 2146–2149.

Massudi, H., Grant, R., Braidy, N., Guest, J., Farnsworth, B., and Guillemin, G.J. (2012). Age-associated changes in oxidative stress and NAD+ metabolism in human tissue. PLoS ONE *7*, e42357.

Mills, K.F., Yoshida, S., Stein, L.R., Grozio, A., Kubota, S., Sasaki, Y., Redpath, P., Migaud, M.E., Apte, R.S., Uchida, K., et al. (2016). Long-Term Administration of Nicotinamide Mononucleotide Mitigates Age-Associated Physiological Decline in Mice. Cell Metab. *24*, 795–806.

Munné, S., Sandalinas, M., Escudero, T., Márquez, C., and Cohen, J. (2002). Chromosome mosaicism in cleavage-stage human embryos: evidence of a maternal age effect. Reprod. Biomed. Online *4*, 223–232.

Nishizuka, Y., and Hayaishi, O. (1963). Studies on the Biosynthesis of Nicotinamide Adenine Dinucleotide. I. Enzymic Synthesis of Niacin Ribonucleotides from 3-Hydroxyanthranilic Acid in Mammalian Tissues. J. Biol. Chem. *238*, 3369–3377.

North, B.J., Rosenberg, M.A., Jeganathan, K.B., Hafner, A.V., Michan, S., Dai, J., Baker, D.J., Cen, Y., Wu, L.E., Sauve, A.A., et al. (2014). SIRT2 induces the checkpoint kinase BubR1 to increase lifespan. EMBO J. *33*, 1438–1453.

National Perinatal Epidemiology and Statistics Unit (2016). Assisted Reproductive Technology in Australia and New Zealand 2016 (UNSW Sydney).

O'Neill, C. (1997). Evidence for the requirement of autocrine growth factors for development of mouse preimplantation embryos *in vitro*. Biol. Reprod. *56*, 229–237.

Okuno, E., and Schwarcz, R. (1985). Purification of quinolinic acid phosphoribosyltransferase from rat liver and brain. Biochim. Biophys. Acta *841*, 112–119.

Peck, B., Chen, C.Y., Ho, K.K., Di Fruscia, P., Myatt, S.S., Coombes, R.C., Fuchter, M.J., Hsiao, C.D., and Lam, E.W. (2010). SIRT inhibitors induce cell death and p53 acetylation through targeting both SIRT1 and SIRT2. Mol. Cancer Ther. *9*, 844–855.

Piacente, F., Caffa, I., Ravera, S., Sociali, G., Passalacqua, M., Vellone, V.G., Becherini, P., Reverberi, D., Monacelli, F., Ballestrero, A., et al. (2017). Nicotinic Acid Phosphoribosyltransferase Regulates Cancer Cell Metabolism, Susceptibility to NAMPT Inhibitors, and DNA Repair. Cancer Res. *77*, 3857–3869.

Preiss, J., and Handler, P. (1958a). Biosynthesis of diphosphopyridine nucleotide. I. Identification of intermediates. J. Biol. Chem. *233*, 488–492.

Preiss, J., and Handler, P. (1958b). Biosynthesis of diphosphopyridine nucleotide. II. Enzymatic aspects. J. Biol. Chem. *233*, 493–500.

Qiu, D., Hou, X., Han, L., Li, X., Ge, J., and Wang, Q. (2018). Sirt2-BubR1 acetylation pathway mediates the effects of advanced maternal age on oocyte quality. Aging Cell *17*, e12698.

Rajman, L., Chwalek, K., and Sinclair, D.A. (2018). Therapeutic Potential of NAD-Boosting Molecules: The *In Vivo* Evidence. Cell Metab. *27*, 529–547.

Rehman, A.U., Anwer, A.G., Gosnell, M.E., Mahbub, S.B., Liu, G., and Goldys, E.M. (2017). Fluorescence quenching of free and bound NADH in HeLa cells determined by hyperspectral imaging and unmixing of cell autofluorescence. Biomed. Opt. Express *8*, 1488–1498.

Riepsamen, A., Wu, L., Lau, L., Listijono, D., Ledger, W., Sinclair, D., and Homer, H. (2015). Nicotinamide impairs entry into and exit from meiosis I in mouse oocytes. PLoS ONE *10*, e0126194.

Riris, S., Webster, P., and Homer, H. (2014). Digital multiplexed mRNA analysis of functionally important genes in single human oocytes and correlation of changes in transcript levels with oocyte protein expression. Fertil. Steril. *101*, 857–864.

Sauer, M.V. (2015). Reproduction at an advanced maternal age and maternal health. Fertil. Steril. *103*, 1136–1143.

Schindelin, J., Arganda-Carreras, I., Frise, E., Kaynig, V., Longair, M., Pietzsch, T., Preibisch, S., Rueden, C., Saalfeld, S., Schmid, B., et al. (2012). Fiji: an open-source platform for biological-image analysis. Nat. Methods *9*, 676–682.

Tatone, C., Di Emidio, G., Barbonetti, A., Carta, G., Luciano, A.M., Falone, S., and Amicarelli, F. (2018). Sirtuins in gamete biology and reproductive physiology: emerging roles and therapeutic potential in female and male infertility. Hum. Reprod. Update *24*, 267–289.

Tian, W.N., Braunstein, L.D., Pang, J., Stuhlmeier, K.M., Xi, Q.C., Tian, X., and Stanton, R.C. (1998). Importance of glucose-6-phosphate dehydrogenase activity for cell growth. J. Biol. Chem. *273*, 10609–10617.

Touati, S.A., Buffin, E., Cladière, D., Hached, K., Rachez, C., van Deursen, J.M., and Wassmann, K. (2015). Mouse oocytes depend on BubR1 for proper chromosome segregation but not for prophase I arrest. Nat. Commun. *6*, 6946.

Trammell, S.A., Schmidt, M.S., Weidemann, B.J., Redpath, P., Jaksch, F., Dellinger, R.W., Li, Z., Abel, E.D., Migaud, M.E., and Brenner, C. (2016). Nicotinamide riboside is uniquely and orally bioavailable in mice and humans. Nat. Commun. *7*, 12948.

Vaziri, H., Dessain, S.K., Ng Eaton, E., Imai, S.I., Frye, R.A., Pandita, T.K., Guarente, L., and Weinberg, R.A. (2001). hSIR2(SIRT1) functions as an NAD-dependent p53 deacetylase. Cell *107*, 149–159.

Vidal, M., and Amigo, J.M. (2012). Pre-processing of hyperspectral images. Essential steps before image analysis. Chemometr. Intell. Lab. Syst. *117*, 138–148.

Wang, Y.P., Zhou, L.S., Zhao, Y.Z., Wang, S.W., Chen, L.L., Liu, L.X., Ling, Z.Q., Hu, F.J., Sun, Y.P., Zhang, J.Y., et al. (2014). Regulation of G6PD acetylation by SIRT2 and KAT9 modulates NADPH homeostasis and cell survival during oxidative stress. EMBO J. *33*, 1304–1320.

Wu, L.E., Meoli, C.C., Mangiafico, S.P., Fazakerley, D.J., Cogger, V.C., Mohamad, M., Pant, H., Kang, M.J., Powter, E., Burchfield, J.G., et al. (2014). Systemic VEGF-A neutralization ameliorates diet-induced metabolic dysfunction. Diabetes *63*, 2656–2667.

Yahata, N., Yuasa, S., and Araki, T. (2009). Nicotinamide mononucleotide adenylyltransferase expression in mitochondrial matrix delays Wallerian degeneration. J. Neurosci. *29*, 6276–6284.

Yeo, C.X., Gilchrist, R.B., Thompson, J.G., and Lane, M. (2008). Exogenous growth differentiation factor 9 in oocyte maturation media enhances subsequent embryo development and fetal viability in mice. Hum. Reprod. *23*, 67–73.

Yoshino, J., Mills, K.F., Yoon, M.J., and Imai, S. (2011). Nicotinamide mononucleotide, a key NAD(+) intermediate, treats the pathophysiology of diet- and age-induced diabetes in mice. Cell Metab. *14*, 528–536.

Zhang, L., Hou, X., Ma, R., Moley, K., Schedl, T., and Wang, Q. (2014). Sirt2 functions in spindle organization and chromosome alignment in mouse oocyte meiosis. FASEB J. *28*, 1435–1445.

Zhang, J., Fang, L., Lu, Z., Xiong, J., Wu, M., Shi, L., Luo, A., and Wang, S. (2016). Are sirtuins markers of ovarian aging? Gene *575*, 680–686.

Zhu, C.T., and Rand, D.M. (2012). A hydrazine coupled cycling assay validates the decrease in redox ratio under starvation in *Drosophila*. PLoS ONE *7*, e47584.

STAR★METHODS

KEY RESOURCES TABLE

Where possible, we have listed resources using RRID numbers from the SciCrunch database.

REAGENT or RESOURCE	SOURCE	IDENTIFIER
Antibodies		
Alexa Fluor 546-labeled goat anti-human	Invitrogen	RRID:AB_2535745
Alexa Fluor 488-labeled goat anti-mouse	Invitrogen	RRID:AB_2534069
Human anti-centromere antibodies (ACA)	Immunovision	RRID:AB_2744669
mouse anti-β-tubulin	Sigma	RRID:AB_2827403
SIRT2	Sigma	RRID:AB_1079981
SIRT1	Cell Signaling Technologies	RRID:AB_2617130
Actin	Millipore	RRID:AB_2223041
HRP conjugated goat anti-rabbit IgG	Bio-Rad	RRID:AB_11125143
HRP conjugated goat anti-mouse IgG	Bio-Rad	RRID:AB_11125547
NMNAT1	Santa Cruz	RRID:AB_2153131
NMNAT3	Santa Cruz	RRID:AB_2819344
Chemicals, Peptides, and Recombinant Proteins		
Hoescht 33342 (bis-benzimide 33342)	Sigma-Aldrich, Australia	99403
ECL Prime chemiluminescence detection system	GE Healthcare	RPN2232
Nicotinamide mononucleotide	GeneHarbor Biotechnologies, Hong Kong	n/a
Pregnant mare's serum gonadotrophin (Folligon)	MSD Animal Health, Australia Intervet, Boxmeer, Holland	
Triton X-100	Sigma-Aldrich, Australia	T8787
3-isobutyl-1-methylxanthine	Sigma-Aldrich, Australia	I7018
Paraffin oil	EMD Millipore, Australia	ES-005-C
M2 media	Sigma Aldrich, Australia	M7167
Bovine serum albumin	Sigma Aldrich, Australia	
Monastrol	Sigma	M8515
Sytox Green nucleic acid stain	Invitrogen	S7020
HEPES-buffered α-minimum essential medium	GIBCO Life Technologies, Grand Island, NY	
human chorionic gonadotrophin	Chorulon, MSD Animal Health, Australia	
5-(and-6)-Chloromethyl-2′,7'-dichlorodihydrofluorescein diacetate (CM-H2DCFDA)	Invitrogen	C6827
Wash media (Research Wash)	IVF vet solutions (Adelaide, Australia)	
Cleavage media (Research Cleave)	IVF vet solutions (Adelaide, Australia)	
Experimental Models: Organisms/Strains		
C57BL6/JAusb mice	Australian BioResources, Moss Vale	RRID:MGI:6200612
SwissTacAusb mice	Australian BioResources, Moss Vale	
SIRT2 transgenic mice B6.Cg-*Col1a1*$^{tm1(CAG-Sirt2)Jmi}$/DsinJ), strain #029604	Jackson Laboratory	RRID:IMSR_JAX:029604
SIRT2 knockout mice (B6.129-*Sirt2*$^{tm1.1Fwa}$/J), strain #012772	Jackson Laboratory	RRID:IMSR_JAX:012772
NMNAT1 transgenic mice	Obtained under material transfer agreement from NCPP, Japan.	RRID:IMSR_RBRC03166
NMNAT3 transgenic mice	Obtained under material transfer agreement from NCPP, Japan.	RRID:IMSR_RBRC03167
Software and Algorithms		
NIS-Elements C acquisition and analysis software	Nikon, Japan	
ImageJ Fiji software		RRID:SCR_002285

(*Continued on next page*)

Continued

REAGENT or RESOURCE	SOURCE	IDENTIFIER
Xcalibur software version 2.2, 2011	ThermoFisher Scientific, Waltham MA	RRID:SCR_014593
G*Power 3.1	Heinrich Heine Universität Düsseldorf	RRID:SCR_013726
Prism v8.1.2	GraphPad	RRID:SCR_002798
Other		
A1 MP+ multiphoton confocal microscope	Nikon, Japan	
glass bottom 35 mm confocal dish	MatTek Corp.	
TSQAccess mass spectrometer	ThermoFisher Scientific, Waltham MA	
Prime 95B cMOS microscopy camera (multispectral imaging)	Photometrics	
FluoroMax Plus-C fluorimeter (multispectral imaging microscope calibration)	Horiba	
Chow diet (mouse feed)	Gordon's Specialty Stock Feeds, Yanderra, NSW, Australia	
Accu-check (hand-held glucose meter)	Roche	
EchoMRI (quantitative MRI, body composition)	EchoMRI, Houston TX, USA	
VisualSonics Vevo 2100 Ultrasound	VisualSonics	RRID:SCR_015816

LEAD CONTACT AND MATERIALS AVAILABILITY

Further information and requests for resources and reagents should be directed to and will be fulfilled by the Lead Contact, Lindsay Wu (lindsay.wu@unsw.edu.au). This study did not generate any new unique reagents. We obtained NMNAT1 and NMNAT3 transgenic mouse lines from the lab of Toshiyuki Araki under an MTA from NCCP Japan, and will share these strains pending permission from NCCP Japan for each request.

EXPERIMENTAL MODEL AND SUBJECT DETAILS

Transgenic and wild-type mouse (*Mus musculus*) strains were bred at Australian Bio-Resources (ABR) in Moss Vale, NSW Australia and delivered to UNSW Sydney at 6-7 weeks of age. Animals were maintained in individually ventilated cages at 22°C at 80% humidity at a density of up to 5 per cage, with *ad libitum* access to food and water. All water in this animal house was acidified to pH 3 with HCl to decrease microbial growth. The UNSW animal house maintained a 12 hr light/dark cycle with lights on at 0700 and off at 1900. With the exception of SwissTacAusb mice used in Figure 2C, animals were on the C57BL/6JAusb background. The ages of animals in each experiment can be found in figure legends. Experiments were carried out with prior approval of the UNSW Animal Care and Ethics Committee (ACEC) under ACEC numbers 13/134B, 15/134A and 18/133A. UNSW ACEC operates under animal ethics guidelines from the National Health and Medical Research Council (NHMRC) of Australia. The generation of SIRT2, NMNAT1 and NMNAT3 transgenic mouse strains used here were as previously described (North et al., 2014; Yahata et al., 2009).

METHOD DETAILS

Ovarian stimulation, oocyte collection for *in vitro* maturation and spindle assessment (Figures 1 and 2)

To collect germinal vesicle (GV) stage cumulus oocyte complexes (COCs) for counting and for *in vivo* maturation for spindle morphology assessment, both ovaries from each mouse were recovered 44 to 46 hours after ovarian stimulation with 7.5 IU Pregnant mare's serum gonadotropin (PMSG) (MSD Animal Health, Australia), which was administered by intraperitoneal (i.p.) injection. Fat and tissue surrounding the ovaries was carefully and rapidly removed under the microscope. Oocytes were mechanically released from ovaries under M2 medium supplemented with 3 mg/ml bovine serum albumin (BSA) in the presence of the growth inhibitor 3-isobutyl-1-methylxanthine (IBMX) (Sigma Aldrich, Australia) at 50 μM using 27-guage needle. The released oocytes, including cumulus oocyte complexes (COC) and denuded oocytes (DO) in the germinal vehicle (GV) stage were collected by aspirator tubes (Sigma Aldrich) and transferred into another drop of IBMX-M2 media overlayed with paraffin oil (EMD Millipore corporation, USA), which was pre-warmed to 37°C. Oocytes were then counted, and the cumulus cells removed by mechanical disruption with a mouth pipette. Oocytes were then rinsed 3 times in IBMX-free M2 (Sigma Aldrich, Australia) containing 3 mg/ml BSA, following 24 hours pH calibration in 5% CO_2, to wash out the IBMX from oocytes, then transferred into another clean, pH calibrated M16 medium

that was overlayed with oil and returned to the incubator under 37°C in a humidified atmosphere of 5% CO_2 to assess subsequent meiotic development. Meiotic maturation measurements included the rates of germinal vesicle breakdown (GVBD) and first polar body extrusion (PBE). The rates of GVBD were measured by counting the number of oocytes where there was a disappearance of nuclear membranes in the first two hours after release. Oocytes that failed to develop into the GVBD stage after 2 hours were discarded, and the remaining GVBD stage oocytes were then continuously incubated to assess PBE development, indicated by the production of first polar body, in 14 hours, 16 hours and 20 hours afterward.

For immunofluorescence and spindle analysis, oocytes which had achieved polar body extrusion were removed from culture medium and very briefly washed through PHEM solution (60 mM PIPES at pH 6.9, 25 mM HEPES, 10 mM EGTA, 2 mM MgCl2.7H_2O), prior to being pre-permeabilized in 0.25% Triton X-100 (Sigma) in PHEM for 5 s at room temperature to soften the zona pellucida. Oocytes were then fixed in 3.7% paraformaldehyde (Sigma) in PHEM for 20 minutes before being permeabilized for 10 minutes in 0.25% Triton X-100 in PBS. Oocytes were then washed in PBS containing 0.5% Bovine serum albumin (BSA) (Sigma) (wash solution) for 5 minutes at room temperature before being blocked overnight in PBS containing 3% BSA and 0.05% Tween-20 (blocking solution) at 4°C. The following morning, oocytes were allowed to equilibrate to room temperature and were probed with primary antibodies.

For immunolabelling, human anti-centromere antibodies (ACA; 1:40; ImmunoVision) and; mouse anti-β-tubulin (1:800; Sigma) were used to label kinetochores and microtubules, respectively. Following primary antibody incubation, the oocytes were then washed and placed into the following secondary antibodies: Alexa Fluor 546-labeled goat anti-human (1:200; Invitrogen) for detecting ACA; and Alexa Fluor 488-labeled goat anti-mouse (1:200; Invitrogen) for detecting β-tubulin. DNA was labeled using 60 s incubation in Hoechst 33342 (1 μg/ml; bis-benzimide; Sigma) in PBS at RT. Oocytes were then transferred to 1-2 μL micro-drops of PBS under mineral oil in glass bottom dishes for confocal imaging.

Serial Z sections of fixed oocytes were captured at 0.5 μm intervals, to span the entire region of the spindle, using an A1 MP+ multiphoton confocal microscope (Nikon, Japan) equipped with a C-Apochromat 63x/1.4 NA oil immersion objective, and processed using NIS-Elements C acquisition and analysis software (Nikon, Japan). Confocal image stacks were projected and further processed using the imaging software FIJI.

For spindle analyses, oocytes exhibiting barrel-shaped bipolar spindles with well-organized microtubule fibers, along with tightly aligned chromosomes on the metaphase plate, were considered as normal. Disordered spindles and lagging chromosomes were considered as abnormal. In order to blind the investigator to analysis, oocytes were given a color code for each dish for imaging and scoring, these color codes corresponded to a treatment group that was blinded to the investigator until after imaging and scoring.

Monastrol treatment and ploidy assessment

Following in-vitro maturation, MII oocytes were cultured for 2 h in M2 medium (Sigma) containing 100 μM monastrol (Sigma), a kinesin-5 inhibitor used to align chromosomes for investigations of chromosome number and dynamics (Kapoor et al., 2000). Oocytes were then fixed, blocked and immunostained as described in the above section. Kinetochores were detected using human anti-centromere primary antibody (ACA; ImmunoVision), followed by incubation in Alexa Fluor 546-labeled goat anti-human (1:200; Invitrogen). DNA was labeled using 10-minute incubation in a 1:5000 dilution of Sytox Green nucleic acid stain (Invitrogen). Images were acquired at 0.5 μm intervals using the microscope described above and processed using the FIJI software.

To obtain a chromosome count in each oocyte, the Z-projection image was initially analyzed to determine the number of kinetochore pairs. Where there was possible overlap of kinetochores or equivocation, serial confocal sections were analyzed while carefully noting the orientation of the chromosomes. Oocytes with excessive chromosome clumping and those with ambiguous counts were excluded from the final aneuploidy assessment. A single trained observer performed all calculations and ploidy determination. Treatment groups were blinded to the investigator until after ploidy determination, through the use of a color code that corresponded to a treatment group which was blinded to the investigator until after imaging and analysis.

Oocyte collection and confocal imaging – DCFDA staining

To collect mature MII COCs, mice were super-ovulated with an intraperitoneal (i.p.) injection of 10 IU pregnant mare serum gonadotrophin (Folligon; Intervet, Boxmeer, Holland) to stimulate follicle growth, followed by a 10 IU i.p. injection of human chorionic gonadotrophin (hCG; Chorulon, MSD Animal Health, Australia) 46 hr later to induce ovulation. COCs were collected form oviductal ampullae using a 27-guage needle and collected in HEPES-buffered α-minimum essential medium (α-MEM; GIBCO Life Technologies, Grand Island, NY) supplemented with 3 mg/ml bovine serum albumin (BSA; Sigma Aldrich, St Louis, MO) 14 – 16 h after hCG injection.

In order to assess the response of the oxidative stress defense mechanisms of oocytes, intra-oocyte glutathione (GSH) and reactive oxygen species (ROS) levels were assessed using the fluorescent probes 5-(and-6)-Chloromethyl-2′,7′-dichlorodihydrofluorescein diacetate (CM-H_2DCFDA) (Invitrogen). In unchallenged oocytes as shown in Figure 1E, as previously described (Li et al.,

2016), MII oocytes were mechanically stripped of their cumulus cells prior to staining and imaging. Oocytes were incubated in HEPES-buffered buffered α-MEM containing 10 μM CM-H_2DCFDA for 30 mins at 37°C protected from light. Oocytes were washed three times in HEPES-buffered α-MEM medium before transfer into a 2 μL drop of HEPES-buffered α-MEM medium, overlayed with paraffin oil in a glass bottom 35 mm confocal dish (MatTek Corp.). Oocytes were imaged immediately under bright field and fluorescence using a Nikon A1+ confocal microscope using a 20X objective at 37°C. For H_2O_2 challenged oocytes as shown in Figure S1D, GV cumulus oocyte complexes were recovered from PMSG stimulated animals and mechanically denuded, and incubated overnight in α-MEM with 50 μM IBMX in a 5% CO_2 incubator at 37°C. Oocytes were then incubated in HEPES buffered α-MEM with IBMX with the addition of 25 μM H2O2, then washed three times and allowed to recover in HEPES buffered α-MEM with IBMX for 90 min, and stained for 30 min in HEPES buffered α-MEM with IBMX containing 10 μM DCFDA. Oocytes were then washed and imaged immediately by confocal microscopy at 37°C. ROS-induced cleavage of CM-H_2DCFDA to DCF fluorescence was examined using an excitation and emission wavelength of 488 nm and 520 nm. Images were taken under fixed conditions with respect to laser energy, signal detection (gain) and pinhole size. Confocal z stacks of 10 μm thickness with 1 μm increments between slices were recorded at the equatorial plain of the oocytes. Mean relative fluorescence intensities of DCF were measured in a minimum of 25 oocytes per group using ImageJ Fiji software (Schindelin et al., 2012).

IVF and embryo culture

Oocyte developmental competence was evaluated by examining the capacity of oocytes to support preimplantation embryo development following *in vitro* fertilization (IVF). IVF and embryo culture were performed as previously described by Yeo et al. (2008). All IVF media was purchased from IVF Vet Solutions (Adelaide, Australia). Briefly, following stimulation of females with 5 IU (young) or 10 IU (aged) PMSG and hCG, COCs were collected form oviductal ampullae using a 27-guage needle and collected in HEPES-buffered α-minimum essential medium COCs were washed three times in wash media (Research Wash) supplemented with 4mg/ml of BSA and co-incubated with capacitated sperm in fertilization media supplemented with 4mg/ml of BSA for 4h at 37°C with 5% O_2, 6% CO_2 and 89% N_2. Sperm was recovered from hybrid CBB6F1 males > 12 weeks of age. Presumptive zygotes were washed three times in wash media and then once in cleavage media (Research Cleave) supplemented with 4 mg/ml BSA and cultured in drops over-layered with mineral oil at a density of 1 embryo per 2 μl. Fertilization rates and subsequent on-time development were assessed every 24 hours.

In the case of simple defined media growth conditions (Figures 4C–E, S5C, S5G, and S5H), oocytes were collected as above, and then maintained in human tubal fluid supplemented with glutamine and EDTA (HTF-GE) media further was supplemented with 3 mg/ml BSA, which is a minimal essential media that does not contain any hormones or trophic ligands (O'Neill, 1997). Embryos were cultured individually in 10 μL drops to further induce culture stress from diluting autocrine trophic ligands. Embryos were fixed at 92 hr post-fertilization for cell counting.

G6PD activity

GV oocytes from PMSG stimulated animals were recovered from ovaries and mechanically denuded of the cumulus layer via mouth pipetting, and collected into 50 mM Tris-HCl pH 7.44 buffer in a volume of 35 μL with 5 oocytes per sample. The oocytes were lysed following a single freeze-thaw cycle, and spun down at 16,000 g, 4 degrees for 10 minutes to separate cell debris. The supernatant (34 μL) was subjected to measurement for glucose-6-phosphate dehydrogenase (G6PD) activity, which was determined as described previously (Tian et al., 1998). Both 6-phosphogluconate dehydrogenase (6PGD) activity and G6PD+6PGD activity were measured separately, and endogenous G6PD activity was determined by subtracting the 6PGD activity alone from the G6PD+6PGD total enzyme activity value. Each reaction mixture consists of 50 mM Tris-HCl, pH 7.44, 2 mM $NADP^+$ and sample in which G6PD activity was to be measured. Reactions were initiated with the addition of 4 mM G6P + 4 mM 6PGL or 4 mM 6PGL alone and activity was measured using a spectrophotometer at room temperature, in a total volume of 60 μL in a 384 well plate. NADPH production was measured at absorbance 340nm every 30 s, and the rate of NADPH synthesis determined as a unit of AU/hour.

NAD^+ measurements

In Figures 1C and 1D, NAD^+ and NADH were measured by mass spectrometry. Following euthanasia, ovaries were quickly dissected, fat removed, weighed, and snap frozen in liquid nitrogen, followed by storage at −80°C. Ovaries were placed in ice-cold 80% methanol, sonicated on ice for 2 × 30 s, incubated at −30°C for 20 min, and then centrifuged at 14,000 *g* for 10 min at 4°C. The supernatant was collected and spiked with a fixed volume of internal standard mixture (Nicotinamide-d4; β-NADH-d5 diammonium salt; β-NAD-d4, from Toronto Research Chemicals, Canada) and dried down using vacuum centrifugation. Samples were reconstituted in 100 mM NH_4OAc and filtered through a 0.22 μm filter. Metabolites were quantified by LC-MS/MS as described by Bustamante et al. (2017) with minor modifications. Briefly, metabolites were separated on a Phenomenex NH_2 column (150 mm x 2 mm x 3 μm) using a binary solvent gradient consisting of 5 mM NH_4OAc (pH 9.5 adjusted with ammonia) and acetonitrile with a flow rate of 250 μl/min. Metabolites were measured using a using a TSQ Access mass spectrometer (ThermoFisher Scientific, Waltham, MA). Calibration curves of individual metabolites were constructed using the peak area ratios (peak area of the metabolite divided by

peak area of the selected internal standard) of each calibrator versus its concentration. Selected internal standards were as follows: Nicotinamide-d4 for nicotinamide; β-NADH-d5 for NADH; β-NAD-d4 for NAD^+. The concentrations of the endogenous metabolites in the tissue extracts were obtained from these calibration curves. Data were normalized to ovary weight. Spectra were processed and peak areas integrated using Xcalibur software (version 2.2, 2011, ThermoFisher Scientific). Data processing was performed using the LCquan feature of the software. Raw datasets are available on our Mendeley site.

The sample size for NAD measurements by mass spectrometry (above) was determined by power calculations based on pilot results obtained using the previously described $NAD^{\pm}$ cycling method of Zhu and Rand (2012). These power calculations, and the pilot results that informed effect size, are available in the separate Supplemental Information. In these pilot studies, following euthanasia, ovaries were rapidly dissected out of animals and snap frozen in liquid nitrogen, then stored at −80°C. Samples were then homogenized in $NAD^{\pm}$ extraction buffer (10 mM nicotinamide, 50 mM Tris HCl, 0.1% Triton X-100, pH 7.4) by sonication. Samples were then centrifuged at 7,000 g for 5 min at 4°C to remove insoluble debris. Aliquots were taken for later protein assay, and samples were then passed through 10 kDa Amicon filters at 14,000 g, 30 min at 4°C to remove proteins from the sample. Flow-through from these samples containing protein-free metabolites were divided into two aliquots. In order to assess NAD^+ alone, in one of these aliquots HCl was added to 10 mM and the samples heated at 70°C for 30 min – this step degrades NADH, leaving behind NAD^+. Each sample was measured in technical triplicate, with 25 μL sample added to 100 μL ADH cycling mix (0.2 mg/ml alcohol dehydrogenase enzyme, 2% ethanol, 100 mM Tris pH 8.5). Samples were allowed to cycle for 10 min at room temperature, followed by 50 μL addition of an MTT/PMS solution (0.1 mM phenazine methosulfate, 0.8 mM 3-(4,5-Dimethylthiazol-2-yl)-2,5-diphenyltetrazolium bromide), 100 mM Tris-HCl pH 8.5). Plates were then incubated and absorbance was measured at 570 nM every 5 min during the cycling reaction, with the 10 min. time point used for the data presented here. NAD concentrations were extrapolated from a standard curve and normalized to protein concentrations determined by a BCA protein assay.

Hyperspectral imaging

In this work we utilized a fluorescence microscope adapted for multispectral imaging by adding a number of custom-made fluorescent channels (Gosnell et al., 2016a, 2016b; Habibalahi et al., 2019; Rehman et al., 2017) to characterize native fluorescence of oocytes. Images were taken in the following channels listed in the table below. We generated a sequence of autofluorescence images of the same cells in each of these channels at 40 times magnification (40x). To acquire the fluorescence images, a sensitive camera was used (Prime 95B cMOS from Photometrics). The camera was operated below −65°C to reduce sensor-induced noise.

To prepare spectral images for quantitative analysis and spectral unmixing, first, a multistep image preparation procedure was carried out (Gosnell et al., 2016a, 2016b; Mahbub et al., 2017; Vidal and Amigo, 2012). This procedure removes sources of errors, reduces noise and standardizes the spectral images. These steps include (i) image equalization, (ii) denoising, (iii) flattening of background illumination, and (iv) cell segmentation which was reported in detail in our previous studies (Mahbub et al., 2017). Briefly, to equalize the images, the intensity value at each channel is converted into the units of photons per pixel per second (PPS). PPS unite standardizes the images acquired with different acquisition parameters such as camera quantum efficiency and exposure time. Next, to reduce random noises such as spikes and Poissonian noise, a 'threshold limiting window' and wavelet filter were employed, respectively.

Further, two reference multispectral images including water and calibration were captured using our multispectral microscope system at the beginning of each experiment. After denoising, the water image was subtracted from the spectral images to remove the unavoidable autofluorescence signals from the microscope slide, Petri dishes, dirt on sensors etc which forms an additive autofluorescence background contribution to all spectral images. The microscope was calibrated using a fluorimeter (FluoroMax Plus-C, Horiba). To this aim we used the calibration fluid which is a mixture of 30 μM NADH (quantum yield 0.019) and 5μM riboflavin (quantum yield 0.24) with non-zero fluorescent response across all our spectral channels. The fluorescence spectrum of this fluid is measured using a fluorimeter and imaged on the multispectral microscope in all our spectral channels. The fluorescence images of the calibration fluid were then smoothed and associated random noises were minimized. The smoothed spectral images with subtracted water background, were then divided by the calibration fluid image and multiplied by fluorescence response of the calibration fluid measured by fluorometer. This was done on a channel by channel basis. Finally, to perform the unmixing process at a single cell resolution, the cells were isolated manually (segmented) by using their DIC image superimposed on selected autofluorescence images.

In the unmixing process the measured spectral characteristics of the cells were compared to the reference spectra of specific fluorophores to find their abundance. In this study, unmixing was performed sing a linear mixing model (LMM). The LMM describes the fluorescent signal of each pixel is a linear combination of a fraction of endmember component spectra. LMM defines weights associated with the concentration of the molecules corresponding to these component spectra. These concentrations were presented as abundance fractions (Keshava, 2003; Keshava et al., 2000; Keshava and Mustard, 2002) and the Robust Dependent Component Analysis (Mahbub et al., 2017) (RoDECA) algorithm (available at our Mendeley site) was employed to identify the dominant native fluorophores and calculate their relative abundance. All raw datasets are available on our Mendeley site.

Spectral channel	Excitation wavelength (nm)	Emission wavelength (bandwidth) (nm)	Dichroic mirror long pass (nm)	Power at objective(μW)	Exposure time (s)
1	345 ± 5	414 (46)	389	6.0	10
2	345 ± 5	451 (106)	389	6.2	6
3	345 ± 5	575 (59)	552	5.7	10
4	358 ± 5	414 (46)	389	5.2	10
5	371 ± 5	414 (46)	389	6.8	10
6	358 ± 5	451 (106)	389	5.2	10
7	371 ± 5	451 (106)	389	6.9	10
8	358 ± 5	575 (59)	552	6.3	10
9	371 ± 5	575 (59)	552	9.9	10
10	377 ± 5	575 (59)	552	18.6	10
11	437 ± 5	575 (59)	552	28.8	10
12	457 ± 5	575 (59)	552	25.2	10
13	476 ± 5	575 (59)	552	24.1	10
14	358 ± 5	594 (long-pass)	552	6.7	10
15	371 ± 5	594 (long-pass)	552	10.4	10

Spectral specification of channels used in this study

High fat feeding

Animals were maintained on chow or high fat diets as described previously (Wu et al., 2014). Chow diet (Gordon's Specialty Stock Feeds, Yanderra, New South Wales, Australia) comprised 8% calories from fat, 21% calories from protein, and 71% calories from carbohydrate, with total energy density of 2.6 kcal/g. High-fat diet (HFD) was prepared in-house and comprised 45% calories from fat (beef lard), 20% calories from protein, and 35% calories from carbohydrate at a density of 4.7 kcal/g, based on rodent diet D12451 (Research Diets, New Brunswick, NJ, USA).

Offspring studies

Male offspring from the control and NMN only treated groups of the breeding trials shown in Figure 3A were maintained to determine whether maternal NMN exposure adversely impacted offspring health. NMN exposure in the mothers was ongoing in drinking water (2 g/L) from 16 weeks of age, including during mating, pregnancy and lactation. Offspring were weaned onto normal drinking water without NMN, and either standard chow diet or high fat diet. Animals were subjected to body composition analysis and glucose tolerance testing at 10 weeks of age, and behavioral analyses at 5 months of age.

Sucrose Preference Test (SPT)

Sucrose Preference Test is a standard test for assessing anhedonic behavior, a symptom of depression. This test was performed at 5 months of age in male offspring of NMN treated females according to a previous study with some modifications (Maniam and Morris, 2010). Mice were housed individually in separate cages with access to two bottles. Mice were first pre-exposed to sucrose solution (1%, w/v) for 24 h as a training to adapt to the newly introduced sucrose solution. They were given access to 2 bottles (sucrose 1%, tap water). On the second day, food and water were removed for 6 hours before being giving access again to sucrose and water. In order to avoid place preference, the position of the bottles was changed, and mice were given to both 1% sucrose solution and water for 24 h. Sucrose preference was calculated according to the following formula: sucrose preference (%) = sucrose intake (g) / [sucrose intake (g) + water (g)] x 100%

Light/Dark Test

The light/dark test (LDT) is a standard test to assess anxiety-like behavior. This test was conducted during light phase at 5 months of age according to a previous protocol (Maniam and Morris, 2010). The LDT apparatus comprised of bright and dark perspex compartments (24 cm 24 cm 27 cm) connected by a small opening (10 cm 10 cm). The light reading on the floor of the light area was 4000–5000 lux and the dark area was lit between 1 and 10 lux. Mice were gently placed in the light area, facing away from the doorway. The total time spent in light and dark areas were recorded for 5 min. The percentage of time spent in light was calculated using the following formula: % time in light area = time spent in light /[(time spent in dark + time spent in light)].

Glucose tolerance test (GTT)

GTT was as described previously (Wu et al., 2014). Animals were fasted from 0800 on the day of the test. At 1400, baseline blood glucose was assayed using a hand-held glucose testing meter (Accu-Check, Roche) through a scalpel nick less than 1 mm from the tip of the tail, with tails protruding from a small upturned cardboard box used to calm animals. Animals were injected with 25% glucose (i.p. injection) at 2 g/L lean body mass, and glucose was assessed at indicated time points from tail bloods. Lean body mass was assessed by quantitative MRI.

Body composition measurements

Body composition was determined by quantitative MRI using an echoMRI (Houston, TX USA) in conscious animals.

Oral gavage and pharmacodynamics

Animals were administered a single oral gavage of NMN in a volume of 100 μL water per 20 g body mass for a total dose of 500 mg/kg. Animals were euthanased at the indicated time point, and ovaries rapidly dissected, cleared of surrounding adipose tissue, and snap frozen for subsequent analysis of NAD^+ levels.

Breeding trial design

The reproductive capacity of 16-month old SIRT2-Tg mice (n = 8) were compared to that of age-matched wild-type littermates (n = 8). We employed a timed-mating protocol, whereby each breeding round commenced with group-housed female mice being 'scented' using dirty bedding from a male's cage for 3 days. This design allowed for stimulation and synchronization of the females' estrous cycles through the Whitten Effect (Jemiolo et al., 1986). Each female was then placed into an individually-housed proven male breeder's cage in a 1:1 ratio ('co-habitation'). This transfer was made in the evening, in anticipation of night-time ovulation (2). The animal-holding facility default light setting is a 12-hour light/12-hour dark cycle. The following early morning each female would be assessed for the presence of viscous vaginal plug as evidence of copulation and, regardless of plug status, were separated to prevent daytime mating. Females with no plug would be replaced with the same male the following evening to undergo another night of mating. If, following 3 consecutive nights of co-habitation, no plug had been observed, females would be separated and observed for weight gain for 5 days to account for the possibility of missed plugs, before undergoing re-scenting. A female would repeat the current mating round until a positive plug was confirmed. Females with positive plug were considered to have passed that mating round and would be housed separately before undergoing micro-ultrasound (VisualSonics Vevo 2100 Ultrasound) on day 15 post-copulation (pc) to determine pregnancy state, as determined by the presence of a fetal heartbeat. Females that had copulated, as demonstrated by plug presence, but did not fall pregnant would be deemed to have failed that mating round and would commence the next mating round with a different male stud, and so on. The scheme for this experiment is shown in Supplemental Information (Methods S1). The data presented in Figure 3H show the cumulative rate of pregnancy following confirmation of mating as described above.

Taking into account the high prevalence of labor difficulty and maternal cannibalism that was encountered in aged nulliparous mice, we were unable to determine offspring number from each pregnancy in the aged *Sirt2* transgenic cohort.

The breeding trial for NMN treated animals as presented in Figure 2J used a different protocol. In this experiment, untreated 12 month old ex-breeder females were treated with NMN (drinking water, 0.5 or 2 g/L) for 4 weeks, following which a male of proven fertility was introduced on an ongoing basis. Animals were weighed weekly, with weight gain of 5 g indicative of pregnancy. Once noted as pregnant, animals were monitored daily for live births. The date of live birth and number of pups were recorded, following which pups were removed and the male re-introduced for further breeding. The cumulative proportion of animals achieving live births was used as the primary outcome for this study, which lasted for 9 weeks following the introduction of males. NMN treatment continued throughout the breeding trial phase of the study.

QUANTIFICATION AND STATISTICAL ANALYSIS

Prior to conducting studies, power calculations were performed to determine sample size using G*Power 3.1, based on effect sizes observed in preliminary pilot studies.

For all continuous outcomes, datasets were subjected to the D'Augusto & Pearson normality omnibus test. If all groups passed this test, data were analyzed as either a two-tailed Student's t test (2 groups), ANOVA (3 or more groups) or as a two-way ANOVA with a 2x2 study design, between group comparisons made by Tukey's multiple comparison test, as indicated in the text of figure legends. Non-parametric datasets were analyzed by a two-tailed Mann-Whitney U-test (2 groups) or a Kruskal-Wallis test (3 or more groups) with between group comparisons made by Dunn's multiple comparison test. Data were subjected to outlier detection using the ROUT test (Q = 1% as cut-off) prior to analyses. For datasets with binary outcomes, a two-sided Fisher's exact test was used.

All statistical calculations and raw datasets are available on our Mendeley site as .xml files (https://doi.org/10.17632/f27ktnj354.1).

All continuous outcome data are presented as violin plots with median and quartile values indicated by dotted lines.

Statistical analyses were performed using GraphPad Prism version 8.1.2.

DATA AND CODE AVAILABILITY

The datasets and code generated during this study are available at a Mendeley site associated with this paper (https://doi.org/10.17632/f27ktnj354.1). All quantitative datasets have been uploaded to our Mendeley site as .xml files exported from Graphpad Prism. These files include the details and results of associated statistical analysis as described in the previous section. Un-cropped western blots and microscopy images have also been uploaded to this site. Raw data associated with hyperspectral imaging have been uploaded with an associated "read me" file, with summarized readings from each channel for each image also shown as a separate excel spreadsheet. The code used to interpret these data using the RoDECA (Robust Dependent Component Analysis) method have been uploaded as pseudocode.

ADDITIONAL RESOURCES

There are no additional resources associated with this study.